Theoretical prediction of mass transfer coefficients in both gas-liquid and slurry bubble columns

Nedeltchev, S.;

Author's Accepted Manuscript

Theoretical prediction of mass transfer coefficients in both gas-liquid and slurry bubble columns

Stoyan Nedeltchev

Chemical Engineering Science

Cite this article as: Stoyan Nedeltchev, Theoretical prediction of mass transfer coefficients in both gas-liquid and slurry bubble columns, *Chemical Engineering Science*, http://dx.doi.org/10.1016/j.ces.2016.06.047

Theoretical Prediction of Mass Transfer Coefficients in Both Gas-Liquid and Slurry Bubble Columns

Stoyan Nedeltchev

Helmholtz-Zentrum Dresden-Rossendorf, Experimental Thermal Fluid Dynamics Bautzner Landstrasse 400,01328 Dresden, Germany

snn13@gmx.net

Abstract

The gas-liquid contact time has been defined in a new way (bubble surface-to-rate of surface formation) and the range of applicability of the penetration theory in both gas-liquid and slurry bubble columns has been examined. In both reactors, the mass transfer coefficients were predicted successfully not only in the homogeneous regime but also in the heterogeneous regime (superficial gas velocities up to 0.08 ms^{-1}).

The results in the article demonstrate the importance of the geometrical characteristics (length and height) of the oblate ellipsoidal bubbles for the accurate calculation of the contact time and thus the volumetric liquid-phase mass transfer coefficient $k_L a$. The gas-liquid interfacial area has been calculated in both reactors in the classical way, i.e. as a function of the gas holdup and inversely proportional to the Sauter-mean bubble diameter. It was found that in the gas-liquid bubble column (0.095 m in ID) the modified penetration theory was applicable to tap water, 9 organic liquids (decalin, nitrobenzene, 2-propanol, 1,4-dioxane, ethanol (99 %), tetralin, xylene, 1,2-dichloroethane, ethylene glycol) and two liquid mixtures (water-glycol and tetralin-ethanol). Tetralin was aerated with both nitrogen and helium, whereas xylene was aerated with hydrogen and helium. The correction factor introduced by Calderbank (1967) was found useful for improving the $k_L a$ predictions in 1,2-dichloroethane, ethanol (99 %), xylene(-hydrogen) and toluene-ethanol 97.2 %. In the case of a slurry bubble column, the new approach was found applicable (at low solids concentrations) to four different gas-liquid-solid systems: air-tetralin-Al_2O_3, air-water-Al_2O_3, air-water-activated carbon and air-Na_2SO_4-kieselguhr. It is noteworthy that in some cases (air-water-Al_2O_3) the new definition of the contact time was found applicable up to solids concentrations of 6.29 %. In the case of a slurry bubble column, it was found that when the theoretical $k_L a$ value is multiplied by the inverse value of the correction factor the predictions improve with about 5 %.

Finally, in the slurry bubble column the contact time was defined on the basis of the length of the micro-eddies and the k_La values in both air-water-alumina and air-water-activated carbon systems were successfully predicted. This is also a potentially good approach.

Abbreviations: ARE   average relative error, %; ID   inner diameter, m; RE   relative error, %

Keywords: New definition of contact time; Penetration theory applicability; Prediction of mass transfer coefficients; Organic liquids; Gas-liquid bubble columns; Slurry bubble columns

Nomenclature

a	specific gas-liquid interfacial area, m^{-1}
C_s	volumetric solids concentration, dimensionless
d_b	mean bubble diameter, m
d_e	equivalent bubble diameter, m
d_s	Sauter-mean bubble diameter, m
D_L	molecular diffusivity, m^2s^{-1}
e	bubble eccentricity (Eq. (**3**)), dimensionless
h	bubble height (Eq. (**5**)), m
f_c	correction factor (Eq. (**17**)), dimensionless
g	acceleration due to gravity, ms^{-2}
k	fluid consistency index, Pa s^n
k_L	liquid-phase mass transfer coefficient, ms^{-1}
k_La	volumetric liquid-phase mass transfer coefficient, s^{-1}
l	bubble length (Eq. (**4**)), m
l_e	length scale of micro eddies, m
n	flow behavior index, dimensionless
R_{SF}	rate of surface formation, m^2s^{-1}
S_B	bubble surface, m^2
t_c	gas-liquid contact time (Eq. (**1a**)), s
u_b	bubble rise velocity, ms^{-1}
U_g	superficial gas velocity, ms^{-1}

Dimensionless numbers

Eo	Eötvös number, dimensionless
Mo	Morton number (Eq. (**6**)), dimensionless

2

Pe_b bubble Peclet number ($=d_eU_g/D_L$), dimensionless

Re_b bubble Reynolds number (Eq. (**1a**)), dimensionless

Sc Schmidt number ($=v_L/D_L$), dimensionless

Sh_b bubble Sherwood number ($=k_Ld_e/D_L$), dimensionless

Ta Tadaki number (Eq. (**6**)), dimensionless

Greek symbols

γ_{eff} effective shear rate, s^{-1}

ε_g gas holdup, dimensionless

ϵ energy dissipation rate per unit mass, m^2/s^3

μ_L liquid viscosity, Pa s

μ_{eff} effective viscosity, Pa s

v_L liquid kinematic viscosity, m^{2}s^{-1}

v_{SL} slurry kinematic viscosity, m^{2}s^{-1}

ρ_G gas density, kgm^{-3}

ρ_L liquid density, kgm^{-3}

ρ_S solids density, kgm^{-3}

ρ_{SL} slurry density, kgm^{-3}

σ surface tension, Nm^{-1}

1. Introduction

Bubble columns are widely used (due to their simple construction and ease of operation) as multiphase reactors and contactors in chemical, petrochemical, biochemical processes, effluent/waste-water treatment process, flotation, metallurgical operations (leaching of metal ores), etc. As chemical reactors they are utilized in many chemical processes such as oxidation, chlorination, alkylation, carbonylation, carboxylation, hydroformylation, sulphonation, dehydrosulphonation, ammonolysis and ozonolysis, halogenation and hydrohalogenation, polymerization and hydrogenation (Shah et al., 1982). Schumpe et al. (1989) provided a table with some typical reactions performed in bubble columns. The main field of application lies in the absorption processes accompanied by slow chemical reactions.

These gas-liquid reactors are also used in biochemical applications such as fermentation and waste water treatment (waste oxidation) (Braulick et al., 1965) as well as aerobic fermentation processes (Deckwer et al., 1978). In the majority of these applications, the step of gas-liquid mass transfer is important and hence the knowledge of the fractional gas hold-

3

up, gas-liquid interfacial area and the volumetric liquid-phase mass transfer coefficient $k_L a$ are crucial for the reliable design of bubble column reactors.

The wide use of bubble columns as chemical reactors is due to their simplicity in operation, compactness, low operating cost, maintenance cost, lack of moving parts, high durability of catalyst, and good heat and mass transfer characteristics.

Schumpe et al. (1979) studied the reaction of sulphite oxidation in two different bubble columns. Tarmy et al. (1984) mentioned that bubble columns are used in processes such as coal gasification and coal liquefaction. Other processes that utilize bubble columns are gas conversion processes involving the production of liquid fuels from synthesis gas (so-called Fischer-Tropsch process) (Kolbel and Ralek, 1980; Saxena, 1995), synthesis of methanol and other synthetic fuels.

Bubble columns provide reasonable interphase mass transfer rates at low energy input (Deckwer and Schumpe, 1993). Mass transfer across the gas-liquid interphase plays an important role in the majority of gas-liquid reactions. High mass transfer rates are achieved in the case of large interfacial area and strong turbulence at the interface (Schumpe et al., 1979). If only mass transfer and reaction affect the performance and other aspects such as e.g. special selectivity requirements, catalyst sedimentation or heat transfer are of negligible importance, bubble column reactors should be operated in the homogeneous flow regime (Schumpe et al., 1979).

Deckwer et al. (1978) measured higher mass transfer coefficients at the column bottom. The authors argue that increased bubble coalescence takes place in the vicinity of the gas sparger. Deckwer et al. (1978) provided a more sophisticated picture of the complex behavior of gas-liquid dispersions at high interphase mass transfer rates.

Mass transfer from the gas to the liquid phase has a decisive importance for the description of systems involving absorption, chemical reactions and fermentations. The mass transfer rate is proportional to the concentration gradient. The proportionality is expressed in terms of the $k_L a$ value. This parameter is important for the design and scale-up of contactors, chemical reactors and bioreactors. According to Deckwer et al. (1978) the $k_L a$ value is used for a rough estimation of mass transfer efficiency. Deckwer et al. (1983) argue that the evaluation of $k_L a$ is not strongly affected by the liquid-phase dispersion coefficient. However, the dispersion must not be neglected. The formation of bubbles at the gas sparger and the resulting enhanced turbulence usually cause higher mass transfer rates (Deckwer et al., 1983). The $k_L a$ values were found to be spatially dependent (Alvarez-Cuenca et al., 1980; Alvarez-Cuenca and Nerenberg, 1981; Nedeltchev et al., 2003). Deckwer et al. (1983) argue that $k_L a$ is

independent of the liquid velocity. The correlation of Akita and Yoshida (1973) is generally recommended for $k_L a$ estimations in bubble columns with less effective gas spargers (Shah et al., 1982).

Although the available information on the $k_L a$ values in bubble column reactors is substantial, the accurate prediction of $k_L a$ still remains difficult due to the strong dependence of the mass transfer performance on reactor geometry, operating conditions and liquid phase properties. The $k_L a$ values may also depend on the experimental method used for their estimation.

In the case of suppressed mixing (multi-staged columns or columns with static mixers), the interphase mass transfer rates improve. Since bubble columns are characterized with large relative liquid holdup and sufficient mass transfer rates, they are especially well suited for gas-liquid reactions taking place in the slow reaction-absorption regime (Deckwer and Schumpe, 1993).

Three-phase (or slurry) bubble columns have a wide range of industrial applications. Solid particles are used as catalysts, products, materials enhancing mass transfer or as carriers for microorganisms (bacteria, micelles, immobilized enzymes, etc.). For instance, this type of reactors are employed for the chlorination of hydrocarbons, polymerization in suspension, desulphurization of flue gases and single cell fermentation. Slurry bubble columns are often used in industry for catalytic reactions. No general mass transfer correlation exists for the design of slurry bubble columns. Most of the mass transfer studies were based on air-water-glass beads system.

The performance of slurry bubble columns largely depends on the characteristics of the employed particles (dimensions, shape, wetting properties, surface, etc.). In slurry bubble columns the solids are fluidized only by liquid circulation induced by rising gas bubbles.

The developing turbulence, related to gas flow conditions, is decisive for the performance of slurry bubble columns. According to Sauer and Hempel (1987) the produced turbulence intensity in the slurry bubble column exceeds that in the gas-liquid bubble column. The result of the higher turbulence is a smaller stable bubble diameter. Sauer and Hempel (1987) argue that the liquid turbulence is intensified even with smaller particles. An increase in turbulence intensity is only possible up to certain values of solids and gas holdups because the distances between bubbles and particles become very small in the swarm. These distances correspond to the size of micro-eddies.

When heavy solid particles (solids density > 1300 kgm^{-3}) are added, the bubble rise velocity is higher than that in gas-liquid bubble columns. Due to the high solids density, the

5

particle distribution is not uniform. A large part of the solids is weakly fluidized above the gas distributor. Apart from intensive solid-solid interactions, which damp the turbulence, the solid packing offers a considerable resistance to the rising bubbles. This resistance can be overcome only by large bubbles.

The main objective of this paper is to test the applicability of the modified penetration theory for prediction of the mass transfer coefficients in both gas-liquid bubble columns and slurry bubble columns operated with different systems at ambient conditions. For this purpose, a new definition (bubble surface-to-rate of surface formation) of the gas-liquid contact time has been developed. It is noteworthy that the main equation in Higbie's (1935) model has never hitherto been tested with systems of gas bubbles for extreme variations of diffusion coefficients and liquid viscosities.

2. Theoretical prediction of mass transfer coefficients in gas-liquid and slurry bubble columns

Mass transfer occurs through the gas-liquid interface. The mass transfer coefficients and the gas-liquid interfacial area inherently depend on the bed hydrodynamics. The liquid-phase mass transfer coefficient incorporates the effects of the complex liquid flow field surrounding the rising gas bubbles. The interfacial area inherently reflects the system bubble behavior.

Lochiel and Calderbank (1964) predicted the effect of bubble shape (mobile spheres, oblate and prolate spheroids and mobile spherical caps) on mass transfer. They considered the bubbles to be axisymmetric about the axis in the direction of rise. Lochiel and Calderbank (1964) argue that steady-state mass transfer conditions around a mobile bubble become established as soon as the bubble moves through a distance approximately equal to its own equivalent spherical diameter. Unsteady state factors should not therefore influence mass transfer to an important degree unless the bubble size varies appreciably before the time required to set up steady conditions around the original body has elapsed.

Deckwer and Schumpe (1993) mentioned that bubble columns are predominantly used in the slow reaction-absorption regime and gas-side resistances to interphase mass transfer are often negligible, so the $k_L a$ value is sufficient to describe the gas-liquid mass transfer rates. Deckwer and Schumpe (1993) argue that the dependence of $k_L a$ on column diameter exists only for column diameters smaller than 0.6 m. Another dimensionless correlation which incorporates gas viscosity has been proposed by Hikita et al. (1981). It contains a coefficient which is different for electrolyte and non-electrolyte solutions. In their empirical correlation, Öztürk et al. (1987) used as a characteristic length the surface-to-volume mean bubble diameter rather than the column diameter. Empirical dimensionless correlations for $k_L a$

6

prediction have been proposed by Nakanoh and Yoshida (1980), Schumpe and Deckwer (1987) and Suh et al. (1991). Most of the correlations (Akita and Yoshida, 1973, 1974; Shah et al., 1982) for k_La prediction in gas-liquid bubble columns neglect the effect of the liquid height. Zhao et al. (1994) proposed empirical correlations that consider the effect of liquid height on k_La. A semi-theoretical approach based on Higbie's penetration theory and Kolmogoroff's theory of isotropic turbulence has been developed by Kawase et al. (1987).

Only few theoretical correlations for k_La prediction in gas-liquid bubble columns (Nedeltchev et al., 2007) and slurry bubble columns (Nedeltchev et al., 2014), CFD models (Wang and Wang, 2007) or algorithmic predictions based on empirical equations (Lemoine and Morsi, 2005; Lemoine et al., 2008) have been used.

The liquid viscosity plays an important role in the k_La estimation. Since the liquid viscosity increases the mean diameter of the bubbles in the dispersion, thus it reduces k_La. Bigger bubbles are stable in the flow at higher viscosities. Besides, liquid viscosity also decreases liquid diffusivity D_L (Calderbank and Moo-Young, 1961). In the case of oxygen transfer, D_L is proportional to $\mu_L^{-0.57}$ (Öztürk et al., 1987). Liquid viscosity reduces the movement of the layers in the contact between the bubble and the liquid as well as slows down surface renewal.

The performance and efficiency of bubble columns largely depends on the k_La value which is the most important operating variable. A good distribution of the bubbles across the reactor increases the efficiency of the gas flow rate on k_La (Martín et al., 2009).

Schumpe et al. (1979) argue that high superficial gas velocities U_g are unfavorable since under heterogeneous flow conditions the achievable conversions are low and the space-time-yield increases only slightly or remain constant. At higher U_g values the nature of the gas-liquid dispersion is heterogeneous and most of the gas is transported through the column as large (spherical-cap) bubbles. These large bubbles have only a short residence time which leads to a decreased conversion (Schumpe et al., 1979). The authors argue that it is better to select an appropriate reactor diameter in order to ensure an operation in the homogeneous flow regime.

Mass transfer across the gas-liquid interface plays an important role in the majority of gas-liquid reactions. Bubble columns are simple but very effective contactors for gas-liquid reactions since they provide large interfacial area and strong turbulence at the interface.

Detailed knowledge of the motion of gas bubbles in liquids is of interest for the understanding of the mass transfer processing involving the contact of liquids and gas bubbles. Chao (1962) argue that the air bubbles in water are spherical at Reynolds numbers up to 400. At higher Reynolds numbers the bubbles become flattened. At first, oblate spheroidal

bubbles are formed and then spherical-cap bubbles. At higher Reynolds numbers the inertia effect comes into play.

The gas holdup, the gas-liquid interfacial area and the $k_L a$ values are the most important variables governing the bubble column operation. These parameters are frequently used for estimation of the performance of bubble columns. The gas holdup drives the liquid circulation and the multiphase turbulence field, and thus determines to a large extent the gas-liquid interfacial area and the associated mass transfer rates, as well.

If the gas holdup and the gas-liquid interfacial area are enhanced, the volumetric mass transfer rate between the gas and liquid phases will be increased and hence all those reactions which are limited by the interfacial transport rate will be enhanced.

One of the main objectives is to improve the process parameters through enhanced phase holdups, higher specific gas-liquid interfacial area, better heat and mass transfer characteristics, all at higher throughputs. As soon as U_g increases, the complex multiphase turbulence takes over and widespread bubble coalescence leads to the formation of larger bubbles. The latter are more buoyant, have a higher rise velocity, and hence the effective gas holdup in the column tends to level off. In other words, the further enhancement of gas holdup is very marginal and certainly not commensurate with the imposed increase in gas flow rate.

In order to understand entirely the mass transfer rates the bubble hydrodynamics should be considered. Martín et al. (2009) argue that two mechanisms determine the mass transfer rate: bubble oscillations (determining the concentration profiles surrounding the bubbles) and contact area. The sparger type also inflences the $k_L a$ values (Shah et al., 1982). This effect can be related to the stability of the bubbles generated at the orifices.

In the homogeneous flow regime, the size of the bubbles is entirely dictated by the sparger design and physical properties of the gas-liquid phases. In contrast, in the heterogeneous flow regime the role of sparger design diminishes depending upon the column height. In the sparger region, the size of the bubbles changes with respect to height depending upon the coalescence nature of the liquid phase (especially the liquid surface tension), the level of turbulence and bulk motion (Thorat et al., 1998). At the end of the sparger region the bubble attains an equilibrium size. The equilibrium bubble size is governed by the breaking forces due to bulk motion (turbulent and viscous stresses) and the stabilizing force due to surface tension. The height of the sparger region depends upon the difference between the primary and secondary bubble size, the coalescence nature of the liquid phase and liquid circulation in heterogeneous (churn-turbulent) regime.

In general, the k_La value declines with solids concentration (Sauer and Hempel, 1987). The decrease in k_La results from an excessive decrease in the liquid-side mass transfer coefficient k_L. The increase in interfacial area per unit volume by enhanced gas holdup is compensated by an even larger decrease in k_L. This coefficient is reduced by rapidly declining turbulence. The particle induced turbulence enhances the mass transfer across the interface only when the particles are very small or the liquid eddies very powerful, so that the particles can follow without a loss of energy.

High interfacial turbulence (caused by high energy dissipation rates) promotes intensive mass transfer. Interaction of micro-eddies and solid particles leads to an increase of turbulence intensity in the bulk phase. This results in smaller bubbles and thus in gas holdup increase. In contrast, interactions between solid particles and gas bubbles are not sufficient to generate additional turbulence which would enhance mass transfer across the interface. This is only possible by using minute particles or in large reactors with high energy micro-eddies which transfer sufficient energy (Sauer and Hempel, 1987).

Only Godbole et al. (1983) observed an enhancement of k_La on addition of solid particles. The k_La improvement is attributed to the special physical properties of oil shale slurry.

2.1 Modification of the penetration theory

The classical penetration theory is applied with a fundamentally new approach for estimation of the gas-liquid contact time. The penetration theory assumes unsteady-state absorption of a gas by a fluid element adjacent to the surface. The liquid element moves at a uniform velocity from the front of the bubble to the rear as penetration into it occurs. The k_La value is calculated as a product of two separate parameters: the liquid-phase mass transfer coefficient k_L and the gas-liquid interfacial area a. The k_L coefficient is estimated on the basis of the Higbie's (1935) penetration theory for the description of the unsteady state mass transfer process around the gas bubbles:

$$k_L = \sqrt{\frac{4 D_L}{\pi t_c}} \tag{1}$$

In dimensionless form Eq. (1) reads as: $Sh_b = 1.13 Pe_b^{0.5}$. This equation is valid when the bubble Peclet number Pe_b is much higher than 100 and bubble Reynolds number Re_b is much higher than 400. Also when the Schmidt number Sc (measure of the ratio of the thickness of the velocity and concentration boundary layers) is much higher than unity. This condition applies for molecules diffusing in liquid. It is also strictly valid for rigid spherical bubbles. It

should be noted that Calderbank et al. (1970) and Weber (1975) also used the contact time concept to estimate the liquid-phase mass transfer coefficient.

When the bubble diameter becomes larger than 2.5×10^{-3} m the bubble deforms and it changes its shape from spherical to ellipsoidal. Calderbank and Moo-Young (1961) argue that the value of the liquid-phase dispersion coefficient is the major factor which influences the value of the liquid-phase mass transfer coefficient. The authors demonstrated that large bubbles ($>2.5 \times 10^{-3}$ m in diameter) give greater mass transfer coefficients than small bubbles ($<2.5 \times 10^{-3}$ m in diameter). According to Calderbank and Moo-Young (1961) unhindered flow situation is envisaged in Higbie's (1935) model. More specifically, large bubbles are characterized with unhindered flow situation, whereas small bubbles are characterized with hindered flow situation.

During the gas-liquid contact (exposure) time for mass transfer a non-stationary diffusion of the elements in the gas-liquid interface is assumed. The gas-liquid contact time t_c characterizes the residence time of liquid elements at the interface. It is generally unknown, but it can be described by an adequate model. The contact time is usually defined as the time it takes for the bubble to travel a length equal to its diameter. Turbulence also determines the renewal of the fluid layers surrounding the bubbles.

As a rough approximation, Nedeltchev et al. (2007, 2014) assumed that the contact time depends on both bubble surface and the rate of surface formation:

$$t_c = \frac{Bubble\ surface}{Rate\ of\ surface\ formation} \tag{1a}$$

The contact time characterizes the residence time of the micro-eddies (responsible for mass transfer in the liquid film) at the interface, i.e. at the bubble surface. In the classical definition of the contact time, it is represented as a ratio of bubble diameter to bubble rise velocity. Due to this rough estimation of the contact time, it was reported that in some gas-liquid systems the penetration theory is inapplicable.

The calculation of the bubble surface depends on the bubble shape (Painmanakul et al., 2005). An oblate ellipsoidal bubble is characterized by its length l (major axis the ellipsoid) and its height h (minor axis of the ellipsoid). The surface area of the ellipsoid is calculated as follows (Fan and Tsuchiya, 1990; Nedeltchev et al., 2007):

$$S_B = \pi \frac{l^2}{2} \left[1 + \left(\frac{h}{l} \right)^2 \frac{1}{2e} ln \frac{(1+e)}{(1-e)} \right] \tag{2}$$

where e is the bubble eccentricity:

$$e = \sqrt{1 - \left(\frac{h}{l}\right)^2} \quad \dots\dots\dots\dots\dots\dots\dots\dots\dots\dots\dots\dots\dots\dots(3)$$

The calculation of both bubble length l and height h was based on the correlations of Terasaka et al. (2004):

$$l = \frac{d_e}{1.14 Ta^{-0.176}} \quad \dots\dots\dots\dots\dots\dots\dots\dots\dots\dots\dots\dots\dots\dots\dots(4)$$

$$h = 1.13 d_e Ta^{-0.352} \quad \dots\dots\dots\dots\dots\dots\dots(5)$$

where

$$Ta = Re_b Mo^{0.23} = \left(\frac{d_e u_b \rho_L}{\mu_L}\right)\left(\frac{g \mu_L^4}{\rho_L \sigma^3}\right)^{0.23} \quad \dots\dots\dots\dots\dots\dots\dots\dots\dots\dots\dots(6)$$

Eqs. **(4)** and **(5)** are valid in the range 2<*Ta*<6. For higher *Ta* numbers, Terasaka et al. (2004) developed different correlations.

The bubble rise velocity is calculated on the basis of the Mendelson's (1967) correlation:

$$u_b = \sqrt{\frac{2\sigma}{\rho_L d_e} + \frac{g d_e}{2}} \quad \dots\dots\dots(7)$$

This equation is particularly suitable in the case of ellipsoidal bubbles.

Intially, Eqs. **(4)**-**(7)** were calculated on the basis of the Sauter-mean bubble diameter d_s. Then, for oblate ellipsoidal bubbles the equilibrium bubble diameter d_e was calculated as follows (see Nedeltchev et al., 2007):

$$d_e = \left(l^2 h\right)^{1/3} \quad (8)$$

An iteration procedure was run until the values of both l and h from two different iterations became practically the same. This corresponded to identical d_s and d_e values.

The rate of surface formation is a product of both the ellipsoidal bubble circumference and the bubble rise velocity (Higbie, 1935; Nedeltchev et al., 2007):

$$R_{SF} = \pi \sqrt{\frac{l^2 + h^2}{2} - \frac{(l-h)^2}{8}} \, u_b \quad (9)$$

R_{SF} quantifies the formation of interphase between the gas bubble and the liquid film surrounding it.

The ratio of Eq. **(2)** to Eq. **(9)** yields the modified gas-liquid contact time t_c at each U_g value.

11

The gas holdup is a basic measurement of the efficiency of gas-liquid contacting. This parameter along with the Sauter-mean bubble diameter d_s determines the specific gas-liquid interfacial area:

$$a = \frac{6\varepsilon_g}{d_s} \tag{10}$$

The gas-liquid interfacial area per unit volume is directly coupled with the gas holdup. Therefore, both should be coupled in a similar way by superficial gas velocity, solids concentration and density. The interfacial area strongly depends on both the physicochemical properties of the system and geometrical parameters of the contactor as well as its hydrodynamics. Eq. **(10)** is strictly valid for rigid spherical bubbles. Garcia-Ochoa and Gomez (2004) mentioned that the bubble deformation is usually small. The influences of almost all parameters are interrelated which makes the accurate design and scale-up of bubble columns a difficult multi-parameter problem.

The only difference in the application of the above-described approach to both gas-liquid and slurry bubble columns is associated with the estimation of the Sauter-mean bubble diameter d_s in both reactors.

2.2. Estimation of bubble diameter in gas-liquid bubble columns

The Sauter-mean bubble diameter in gas-liquid bubble columns was calculated by means of the correlation of Wilkinson et al. (1994) which is considered the most reliable in the literature on bubble columns:

$$\left(\frac{g\,\rho_L d_s^2}{\sigma} \right) = 8.8 \left(\frac{U_g\,\mu_L}{\sigma} \right)^{-0.04} \left(\frac{\sigma^3 \rho_L}{g\,\mu_L^4} \right)^{-0.12} \left(\frac{\rho_L}{\rho_G} \right)^{0.22} \qquad ..\ldots\ldots\ldots\ldots\ldots.(11)$$

This correlation accounts for the fact that the bubble size decreases with the increase of both superficial gas velocity U_g and operating pressure. According to Deckwer et al. (1978), the mean bubble diameter depends on the turbulence within the gas-liquid dispersion. So, the small decrease of the Sauter-mean bubble diameter with the increase of U_g can be attributed to increasing turbulence.

2.3. Estimation of bubble diameter in slurry bubble columns

The Sauter-mean bubble diameter in slurry bubble columns was calculated by means of the modified correlation of Krishna et al. (1994):

$$d_b^2 = 8.8 \left(\frac{\sigma}{(\rho_L - \rho_G) g} \right) \left(\frac{U_g \, \mu_L}{\sigma} \right)^{-0.04} \left(\frac{\sigma^3 \, \rho_L}{g \, \mu_L^4} \right)^{-0.12} \left(\frac{\rho_L}{\rho_G} \right)^{0.22} \tag{12}$$

In order to adapt this correlation to slurry bubble columns, the liquid density ρ_L was substituted with slurry density ρ_{SL} and the liquid viscosity μ_L with the effective viscosity μ_{eff}.

In the case of slurry bubble columns, the molecular diffusivity D_L was calculated as a function of the effective viscosity:

$$D_L = 5.0 \times 10^{-11} \left(\mu_{eff} \right)^{-0.57} \tag{13}$$

This equation was proposed by Öztürk et al. (1987). In slurry bubble columns the effective viscosities μ_{eff} of non-Newtonian suspensions were calculated from the Ostwald-de Waele correlation:

$$\mu_{eff} = k \, \gamma_{eff}^{n-1} \tag{14}$$

where k is a fluid consistency index and n is a flow behavior index. The effective shear rates for non-Newtonian fluids were calculated by means of the correlation of Schumpe and Deckwer (1987):

$$\gamma_{eff} = 2800 \, U_g \tag{15}$$

The slurry density was calculated as follows:

$$\rho_{SL} = \rho_L (1 - C_s) + \rho_s \, C_s \tag{16}$$

In the calculations of both bubble Reynolds number Re_b and Morton number Mo (see Eq. (6)) the slurry density was used instead of the liquid density and effective viscosity instead of liquid viscosity.

3. Experimental setups and systems used

In both gas-liquid and slurry bubble columns superficial gas velocities U_g up to 0.08 ms^{-1} were investigated. According to the bubble shape diagrams prepared by Clift et al. (1978) and Fan and Tsuchiya (1990) oblate ellipsoidal bubbles were formed under all operating conditions examined.

3.1. $k_L a$ measurements in a gas-liquid bubble column

The $k_L a$ measurements were carried out in a jacketed glass bubble column (0.095 m in ID). The clear liquid height was set at 0.85 m. A single tube ($\varnothing$ 3.0×10^{-3} m) was used as a gas distributor. Air, nitrogen, hydrogen and helium were employed as the gas phase.

13

The k_La values were measured by dynamic oxygen absorption or desorption methods. A complete mixing in the bubble column was assumed. The oxygen fugacity in the liquids was measured with a polarographic oxygen electrode (WTW-EO 90) inserted horizontally at half of the dispersion height. The electrode response time was 3 s in water and shorter in most organic liquids. For absorption runs, oxygen was desorbed by sparging nitrogen. After disengagement of all nitrogen bubbles, a pre-adjusted air flow was fed by switching two magnet valves, and the increase in oxygen fugacity was recorded. For desorption runs, oxygen-free inert gas (nitrogen, hydrogen or helium) was sparged into air-saturated liquid. The application of the penetration theory in the following liquids was investigated: decalin, 1,2-dichloroethane, 1,4-dioxane, ethanol (99 %), nitrobenzene, 2-propanol, ethylenglycol, tetralin, xylene and tap water. Tetralin was aerated with nitrogen and helium, whereas xylene with hydrogen and helium. In addition, the following liquid mixtures were studied: water-glycol (22.4 %; 60.0 % and 80.0 %) and toluene-ethanol (94.3 % and 97.2 %). The physicochemical properties of all these liquids are given in Nedeltchev et al. (2007).

3.2. k_La measurements in a slurry bubble column

The k_La measurements were performed in a slurry bubble column (0.095 m in ID) made of glass. A complete mixing in the slurry bubble column was assumed. The unaerated height of the suspension was kept constant (0.85 m). Air was used as the gas and it was passed through a drying tower and saturator filled with the same liquid and thermostated to the same temperature as the slurry bubble column. The column was operated batchwise with respect to the slurry phase and continuously with respect to the gas phase.

A small single tube ($\varnothing$ 0.9×10^{-3} m) was used as a gas distributor. Air-Na_2SO_4-kieselguhr (diatomaceous earth), air-water-alumina (Al_2O_3) and air-water-activated carbon have been used as slurry systems. In the case of air-tetralin-alumina system, a bigger single tube ($\varnothing$ 3.0×10^{-3} m) has been used as a gas distributor. The physicochemical properties of the liquids and solids used are summarized in Nedeltchev et al. (2014).

The experimental gas holdups ε_g were determined visually from the change in the dispersion height due to the gas flow rate. The k_La values were determined by means of the dynamic oxygen absorption method, i.e. increase of the oxygen fugacity during aeration of the initially oxygen-free liquids. The experimental k_La values were recorded by a fast response polarographic oxygen electrode (WTW EO 90, time constant: 3 s). As recommended by Sauer and Hempel (1987) the oxygen electrode was inserted horizontally at half of the dispersion height above the gas distributor, in order to minimize the influence of the start-up phase,

bubble contact and non-ideal local dispersion. At first, oxygen was desorbed by sparging nitrogen. After the disengagement of the nitrogen bubbles but before any significant sedimentation of the particles, aeration was started by switching two magnet valves. More details are provided elsewhere (Öztürk and Schumpe, 1987).

4. Results and discussion

4.1. Application of the penetration theory in a bubble column equipped with a single tube

Fig. 1 shows the parity plot of $k_L a$ values in five different organic liquids. The mass transfer measurements were performed in a bubble column (0.095 m in ID) equipped with a single-tube sparger (3×10^{-3} m in diameter). It is clear that 48 $k_L a$ values can be predicted successfully by the penetration theory and the new definition (Nedeltchev et al., 2007; Nedeltchev et al., 2014) of the contact time without the introduction of any correction factor. In all five organic liquids, the $k_L a$ values were predicted successfully up to U_g=0.08 ms^{-1}, i.e. not only in the homogeneous regime but also in the heterogeneous regime. It seems that the Sauter-mean bubble diameter d_s (Wilkinson et al., 1994) can be used for prediction of the $k_L a$ values in the churn-turbulent flow regime. It is noteworthy that the $k_L a$ values for 2-propanol and tetralin lie on the + 20 % error line or very close to it since the bubble Reynolds numbers for these two liquids are lower than 400.
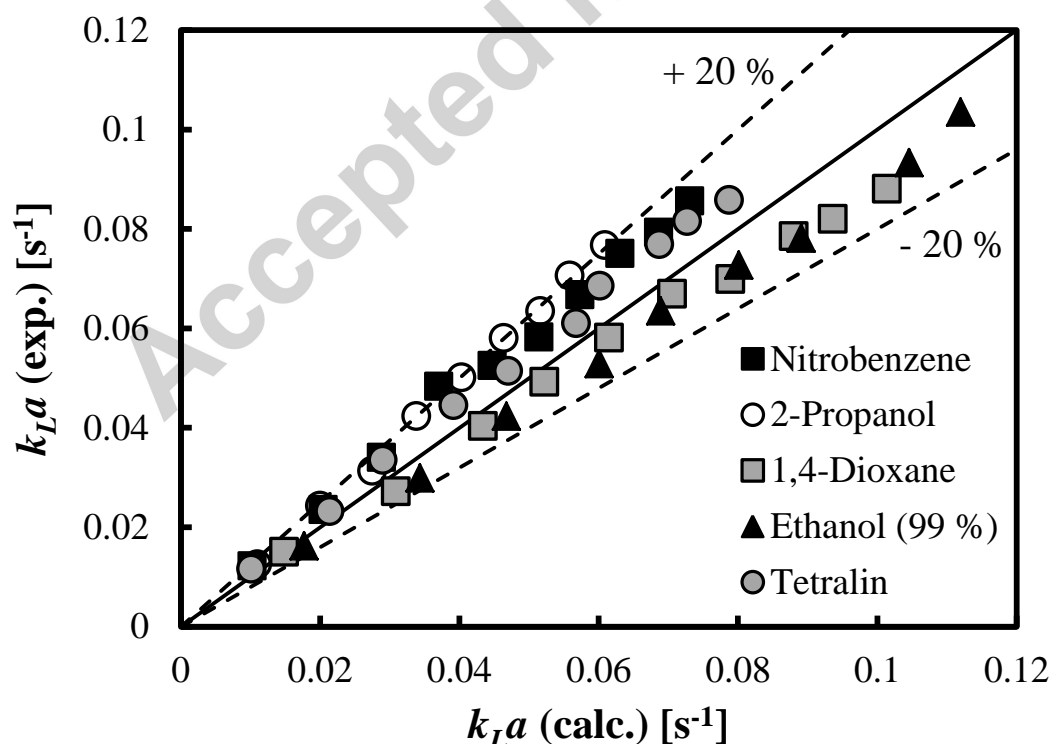

Fig. 1. Parity plot of $k_L a$ values in five organic liquids in a gas-liquid bubble column.

In **Table 1a** and **b** are summarized the ranges of the most characteristic parameters for the application of the penetration theory in the case of these particular five organic liquids.

Table 1a. Bubble size and its geometrical characteristics in five organic liquids.

Liquid	d_s [mm]	l [mm]	h [mm]
1,4-Dioxane	3.670-3.505	4.183-3.962	2.826-2.744
Ethanol (99 %)	3.585-3.424	4.094-3.878	2.750-2.670
Nitrobenzene	4.033-3.852	4.651-4.405	3.033-2.955
2-Propanol	4.137-3.951	4.820-4.588	3.048-2.963
Tetralin	4.388-4.191	5.065-4.797	3.294-3.200

Table 1b. Three important dimensionless numbers in five organic liquids.

Liquid	Re_b [-]	Ta [-]	Eo [-]
1,4-Dioxane	544.232-519.693	4.425-4.226	4.282-3.906
Ethanol (99 %)	434.010-414.164	4.476-4.271	4.557-4.157
Nitrobenzene	452.461-431.242	4.735-4.513	5.090-4.643
2-Propanol	244.835-232.769	5.018-4.770	6.306-5.752
Tetralin	379.600-361.630	4.759-4.533	5.290-4.826

So, it can be concluded that in the case of these particular five organic liquids the penetration theory based on the new definition of the contact time is applicable for bubble sizes not smaller than 3.424×10^{-3} m and not bigger than 4.388×10^{-3} m, bubble Reynolds numbers Re_b in the range 232.769-544.232, Tadaki numbers Ta in the range 4.226-5.018 and Eötvös numbers Eo in the range 3.906-6.306.

Fig. 2 shows that the penetration theory without any correction is also applicable to three additional organic liquids (1,2-dichloroethane, decalin and ethylene glycol), tap water and three organic mixtures between water and glycol. It is worth mentioning that in the case of ethylene glycol the k_La predictions are good only up to U_g=0.051 ms^{-1}. The results in **Tables 2a** and **b** show that the penetration theory is applicable from relatively small bubble sizes (about 3×10^{-3} m) as in the case of 1,2-dichloroethane to relatively large bubble sizes (about 7.5×10^{-3} m) as in the case of ethylene glycol. In the case of tap water, the bubble Reynolds number Re_b can be as high as 1073, whereas in the case of ethylene glycol the Eo number can be as high as 13.
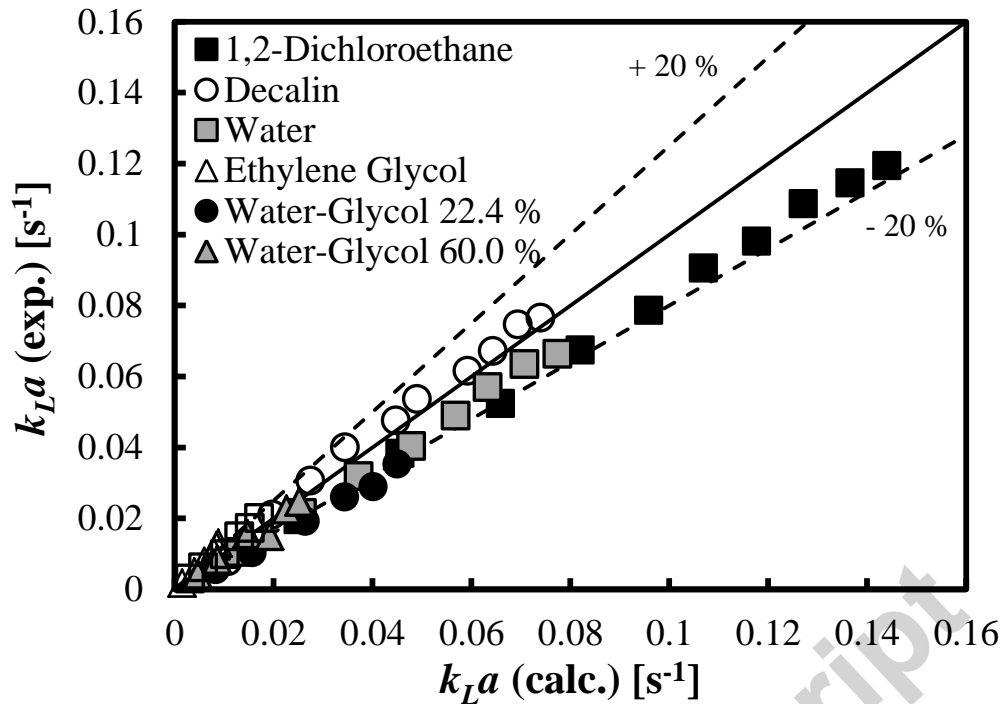
16

Fig. 2. Parity plot of $k_L a$ values in three organic liquids, three liquid mixtures and water in a gas-liquid bubble column.

Table 2a. Bubble size and its geometrical characteristics in three different organic liquids, tap water and different mixtures between water and glycol.

Liquid	d_s [mm]	l [mm]	h [mm]
Decalin	4.498-4.296	5.224-4.946	3.336-3.242
1,2-Dichloroethane	2.946-2.813	3.326-3.151	2.312-2.243
Ethylene glycol	7.447-7.162	9.387-8.905	4.688-4.634
Water	4.651-4.462	5.197-4.953	3.726-3.623
Water-glycol 22.4 %	4.989-4.765	5.728-5.425	3.786-3.677
Water-glycol 60.0 %	5.915-5.649	6.969-6.595	4.262-4.146
Water-glycol 80.0 %	6.567-6.271	7.874-7.447	4.570-4.460

Table 2b. Three important dimensionless numbers in three different organic liquids, tap water and different mixtures between water and glycol.

Liquid	Re_b [-]	Ta [-]	Eo [-]
Decalin	298.842-284.346	4.925-4.686	5.891-5.374
1,2-Dichloroethane	777.922-744.251	4.193-4.012	3.575-3.260
Ethylene glycol	91.036-86.687	6.856-6.528	12.888-11.921
Water	1073.266-1033.437	3.956-3.809	2.944-2.710
Water-glycol 22.4 %	476.580-454.543	4.613-4.400	4.779-4.360
Water-glycol 60.0 %	241.301-229.095	5.346-5.075	7.142-6.514

Water-glycol 80.0 %	160.01-151.510	5.903-5.589	9.133-8.329

Fig. 3 reveals that the prediction of the k_La values in two mixtures between toluene and ethanol, tetralin sparged by both nitrogen and helium as well as xylene sparged by both hydrogen and helium is successful provided that the classical penetration theory is used along with the new definition of the gas-liquid contact time. The differences between the predicted and experimental k_La values are always within ± 20 % error limits.
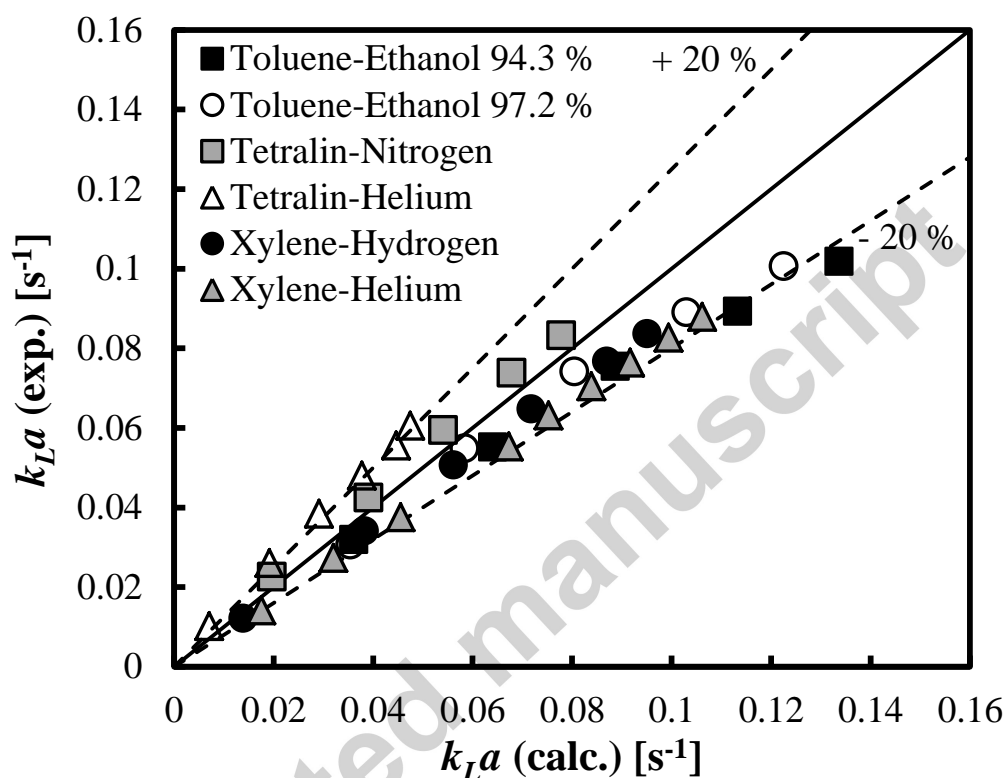

Fig. 3. Parity plot of k_La values in two liquid mixtures, tetralin and xylene operated with nitrogen, hydrogen or helium.

In **Table 3a** are listed the bubble diameters and the main geometric characteristics of the bubbles in two different liquid mixtures, tetralin sparged with both nitrogen and helium and xylene sparged with both hydrogen and helium. The maximum bubble size is 5.44×10^{-3} m, whereas the minimum bubble size is 3.381×10^{-3} m. In **Table 3b** are given the key dimensionless numbers. The penetration theory is applicable in the Re_b range from 362.983 to 1090.164, Ta range from 4.218 to 6.052 and Eo range from 3.992 to 8.137.

Table 3a. Bubble size and its geometrical characteristics in different organic liquids and liquid mixtures.

Liquid	d_s [mm]	l [mm]	h [mm]
Toluene-Ethanol 94.3 %	3.491-3.381	3.968-3.821	2.704-2.648

Toluene-Ethanol 97.2 %	3.495-3.384	3.976-3.828	2.701-2.645
Tetralin (-nitrogen)	4.343-4.206	5.004-4.817	3.273-3.208
Tetralin (-helium)	5.44-5.196	6.551-6.199	3.753-3.652
Xylene (-hydrogen)	4.180-3.990	4.895-4.632	3.049-2.961
Xylene (-helium)	3.980-3.800	4.618-4.427	2.957-2.871

Table 3b. Three important dimensionless numbers in different organic liquids and liquid mixtures.

Liquid	Re_b [-]	Ta [-]	Eo [-]
Toluene-Ethanol 94.3 %	462.598-447.950	4.356-4.218	4.255-3.992
Toluene-Ethanol 97.2 %	445.960-431.659	4.383-4.243	4.339-4.068
Tetralin (-nitrogen)	375.457-362.983	4.707-4.550	5.183-4.861
Tetralin(-helium)	482.739-457.759	6.052-5.739	8.137-7.424
Xylene(-hydrogen)	1090.164-1037.994	5.163-4.916	5.266-4.799
Xylene(-helium)	1035.283-987.095	4.903-4.675	4.774-4.353

In **Table 4** are listed the range of the contact times t_c for the liquids studied as well as the characteristic Schmidt numbers Sc. The lowest t_c is equal to 0.0169 s (in the case of 1,2-dichloroethane), whereas the highest t_c is equal to 0.0383 s (in the case of ethylene glycol). The application of the penetration theory along with the new definition of the contact time is valid for the range of Schmidt numbers between 201.105 (in the case of xylene) and 68 905.937 (in the case of ethylene glycol).

Table 4. Contact times and Schmidt numbers in all liquids studied.

Liquid	t_c [s]	$Sc=v_L/D_L$ [-]
Decalin	0.0251-0.0240	1814.1
1,2-Dichloroethane	0.0178-0.0169	248.9
1,4-Dioxane	0.0210-0.0199	640.3
Ethanol (99 %)	0.0210-0.0200	634.8
Ethylene glycol	0.0383-0.0369	68 905.9
Nitrobenzene	0.0230-0.0219	1030.1
2-Propanol	0.0245-0.0234	2140.8
Tetralin (-nitrogen)	0.0239-0.0232	1425.4
Tetralin(-helium)	0.0299-0.0286	1425.3
Toluene-Ethanol 94.3 %	0.0204-0.0197	553.7
Toluene-Ethanol 97.2 %	0.0205-0.0198	584.4

Water	0.0211-0.0201	480.0
Water-glycol 22.4 %	0.0252-0.0240	1473.1
Water-glycol 60.0 %	0.0301-0.0288	6226.3
Water-glycol 80.0 %	0.0334-0.0320	15171.7
Xylene(-hydrogen)	0.0238-0.0227	201.1
Xylene(-helium)	0.0226-0.0215	201.1

4.1.1. Role of the correction factor in gas-liquid bubble columns

It was found that the correction factor for oblate ellipsoidal bubbles derived by Lochiel and Calderbank (1964), Calderbank (1967) and Calderbank et al. (1970)

$$f_c = \sqrt{1 - \frac{2.96}{(Re_b)^{0.5}}} \qquad (17)$$

can be used for improving the $k_L a$ predictions. The bubble Reynolds number Re_b is defined in Eq. **(6)**.

The multiplication of the theoretically predicted $k_L a$ value with the correction factor f_c (see Eq. **(17)**) decreases the difference between the experimental and predicted $k_L a$ values. In **Fig. 4** is shown the $k_L a$ parity plot for 1,2-dichloroethane in the cases with and without correction factors. One can see clearly that the usage of the correction factors improves the $k_L a$ predictions. The average relative error (ARE) without the correction factors is 21.1 %, whereas the ARE with the correction factors is 5.9 %. In **Fig. 4** the open circles at all U_g values lie practically on the central (error-free) line.
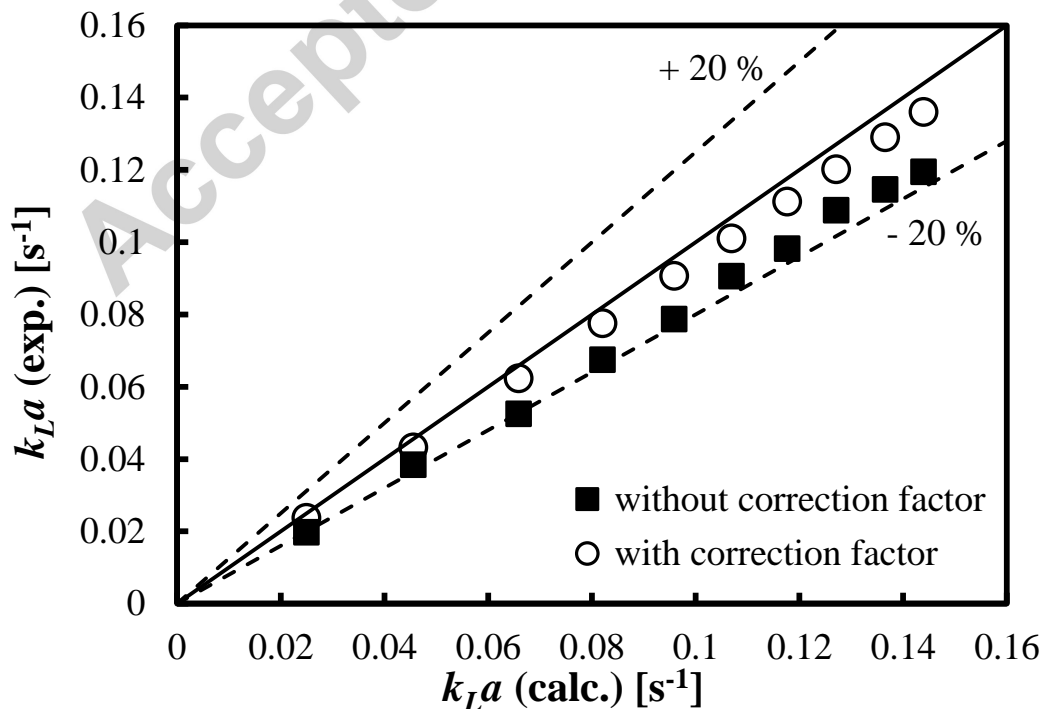
Fig. 4. Parity plot of k_La values (with and without correction factors) in 1,2-dichloroethane.

Fig. 5 shows that in the case of the ethanol (99 %) the usage of the correction factor (as defined by Eq. **(17)**) leads to improved k_La predictions. The average relative error decreases down to 2.68 %.
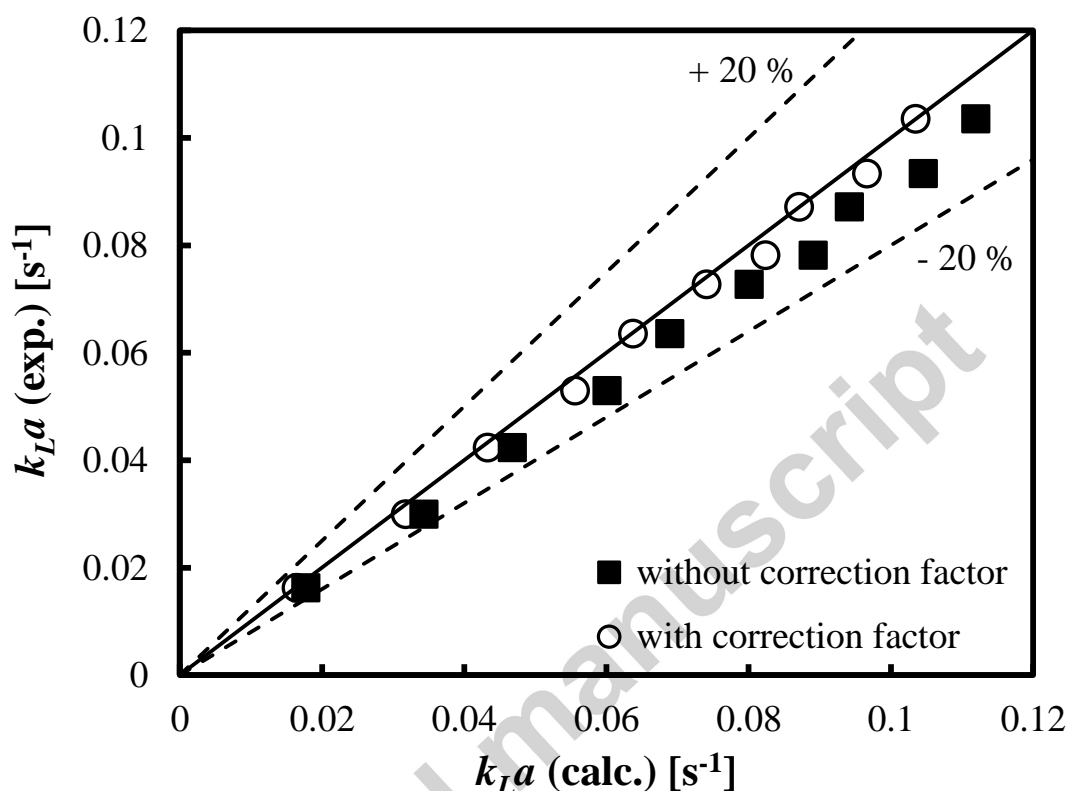

Fig. 5. Parity plot of k_La values (with and without correction factors) in ethanol (99 %).

Fig. 6 shows the improvement in the k_La prediction in the case of xylene(-hydrogen) when the correction factor from Eq. **(17)** is used. The average relative errors (see **Table 5**) reveal that the improvement of the k_La prediction is more than 5 %.

Fig. 7 and the ARE results for toluene-ethanol 97.2 % mixture in table 5 demonstrate that the correction factor is also useful in this particular case. The open circle keys lie much closer to the error-free (central) line.

It is noteworthy that for all 4 cases presented in Figs. 4-7 the bubble Reynolds numbers Re_b are higher than 400, i.e. Eq. (1) is strictly valid.
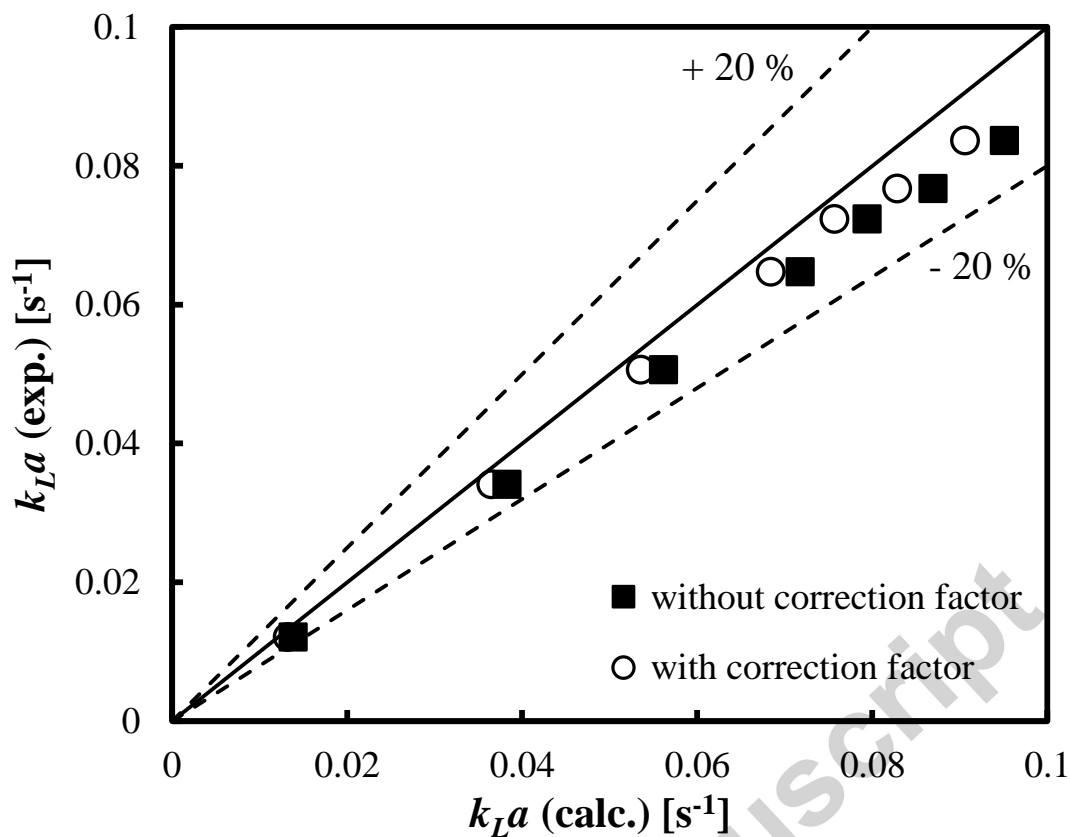
Fig. 6. Parity plot of k_La values (with and without correction factors) in xylene(-hydrogen).
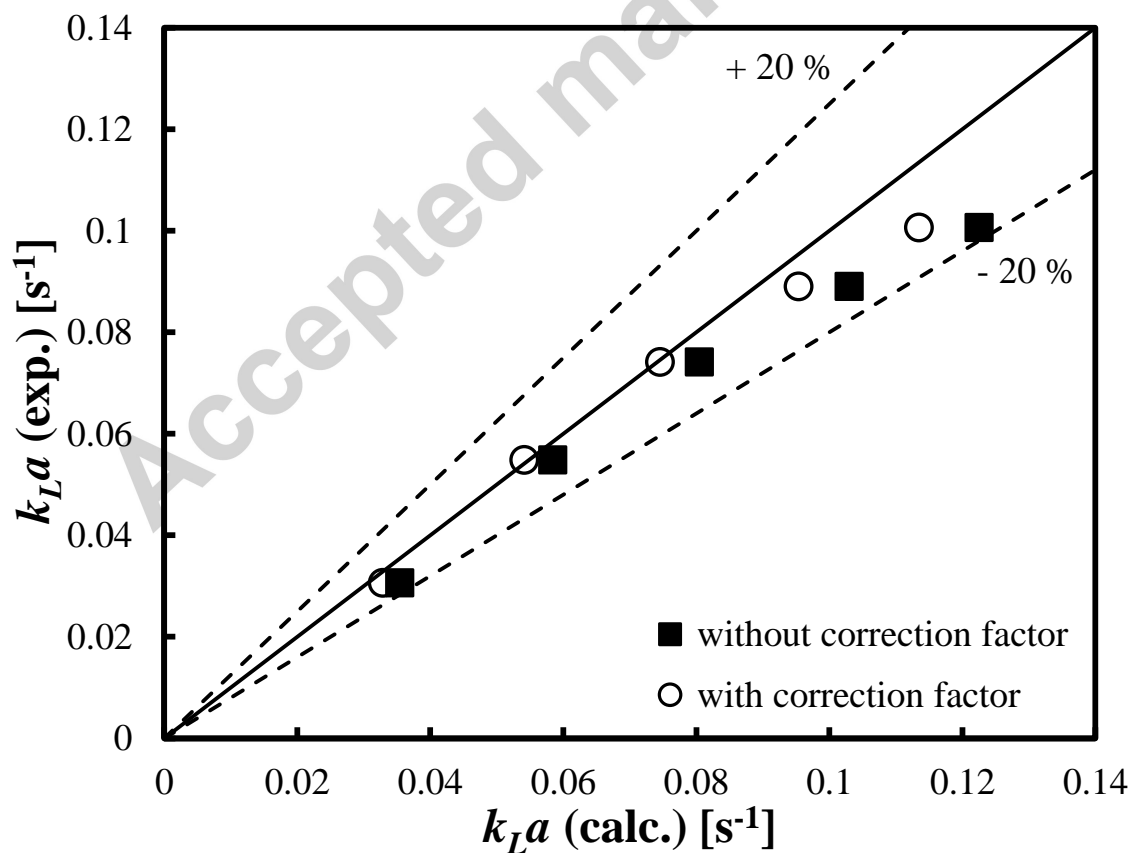

Fig. 7. Parity plot of k_La values (with and without correction factors) in toluene-ethanol 97.2 % mixture.

Table 5 shows that in most liquids studied the correction factor f_c improves the k_La predictions. The f_c values in the selected liquids vary in between 0.924 and 0.954. This means that the deviation from the perfect spherical shape is not more than 10 %.

Table 5. Description of the f_c ranges and the average relative errors (AREs) of the k_La values in some liquids predicted with and without correction factors.

Liquid	f_c range	ARE (with f_c)	ARE (without f_c)
1,2-Dichloroethane	0.9454-0.9442	5.86 %	21.08 %
1,4-Dioxane	0.9344-0.9328	4.17 %	9.43 %
Ethanol (99 %)	0.9262-0.9244	2.68 %	11.00 %
Toluene-Ethanol 94.3 %	0.9286-0.9274	12.37 %	21.11 %
Toluene-Ethanol 97.2 %	0.9273-0.9260	5.85 %	13.72 %
Water	0.9538-0.9529	11.53 %	17.01 %
Water-glycol 22.4 %	0.9297-0.9280	29.91 %	39.87 %
Xylene(-helium)	0.9529-0.9518	15.04 %	20.82 %
Xylene(-hydrogen)	0.9541-0.9530	7.00 %	12.24 %

4.2. Application of the penetration theory in a slurry bubble column equipped with a single tube

The penetration theory based on the new definition of gas-liquid contact time (Eq. **(1a)**) is applicable also to slurry bubble columns. **Fig. 8** shows that in the case of air-tetralin-alumina system up to solids concentrations of 4.33 % and superficial gas velocities U_g of 0.077 ms^{-1} the prediction of the k_La values (36 different conditions) is successful. It is noteworthy that the experimental k_La values are slightly higher than the theoretically predicted ones. This means that the new formulation of the penetration model covers not only the homogeneous regime but also the heterogeneous regime. The bubble size, slurry density and effective viscosity were calculated by means of the equations described in section 2.3.
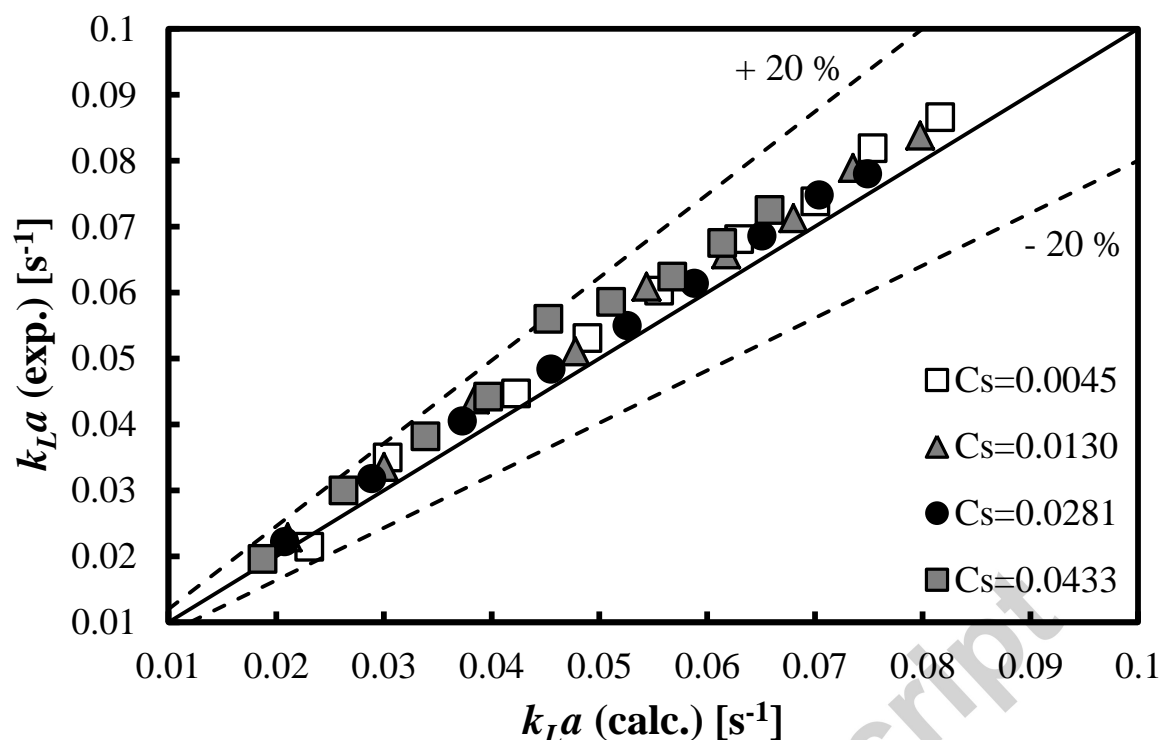
Fig. 8. Parity plot of $k_L a$ values in a slurry bubble column operated with air-tetralin-Al_2O_3 system.

The approach is also applicable to the air-water-activated carbon system up to solids concentrations C_s of 5.11 %. **Fig. 9** shows that at each C_s value the modified penetration model predicted the $k_L a$ values successfully up to U_g values of 0.072 ms^{-1}, i.e. the model is applicable in the three main flow regimes. At C_s=0.0256 and 0.0511 the difference between experimental and predicted $k_L a$ values at U_g=0.064 and 0.072 ms^{-1} (the last two $k_L a$ values at both C_s) deviates from the $k_L a$ fit at lower U_g values. The last two points at C_s=0.0256 and 0.0511 correspond to the churn-turbulent flow regime.
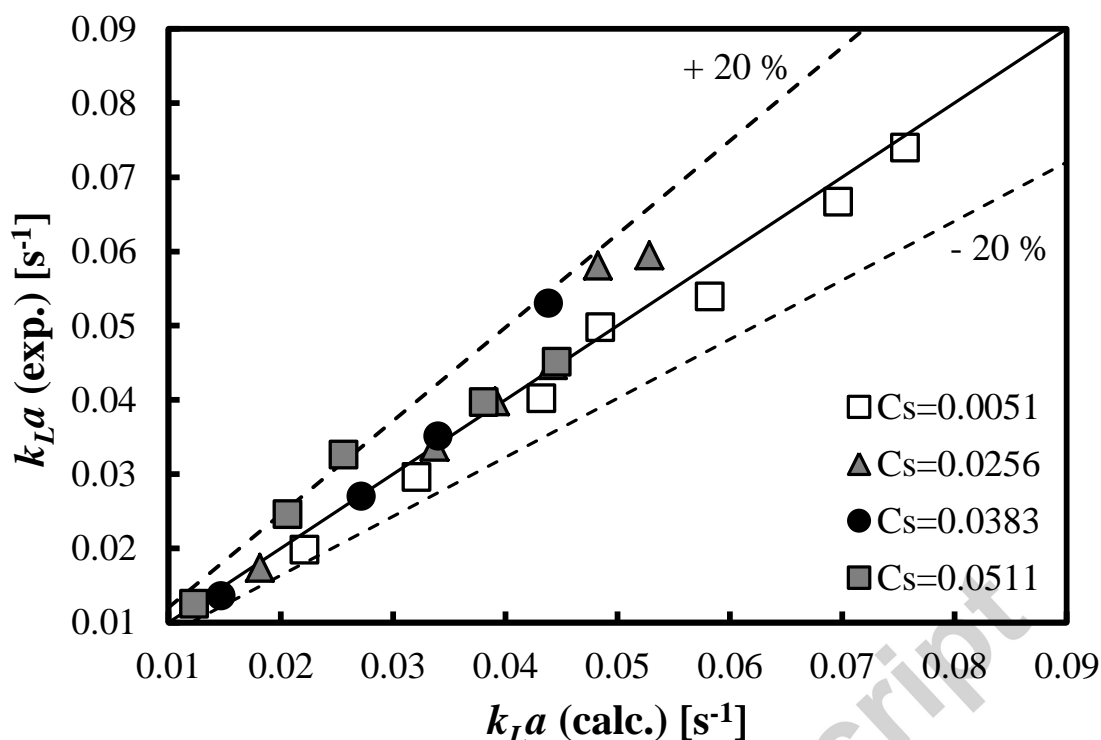
Fig. 9. Parity plot of k_La values in a slurry bubble column operated with air-water-activated carbon system.

Fig. 10 shows that the penetration theory is applicable without any correction to the system air-water-alumina. In this particular case, the k_La data were successfully fitted up to solids concentrations C_s of 6.3 %. Again, the approach is applicable up to superficial gas velocities of 0.072 ms^{-1}. It is noteworthy that at C_s=0.0314 the k_La predictions are outside the error limits (± 20 %) but at higher C_s values the k_La fit improves again.

In the case of the system air-Na$_2$SO$_4$-kieselguhr the penetration theory yields good results at superficial gas velocities exceeding the first transition velocity. In **Fig. 11** are shown the successful k_La predictions at different solids concentrations C_s. The k_La predictions are always lower than the experimental values.
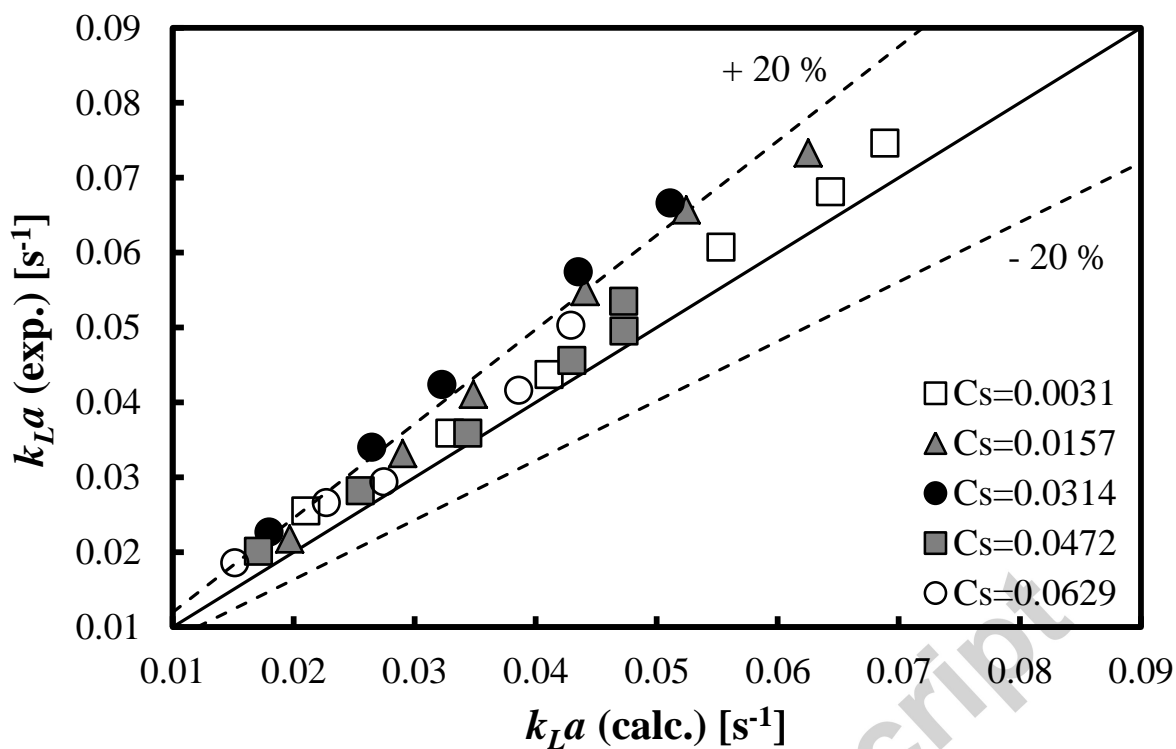
Fig. 10. Parity plot of k_La values in a slurry bubble column operated with air-water-alumina system.
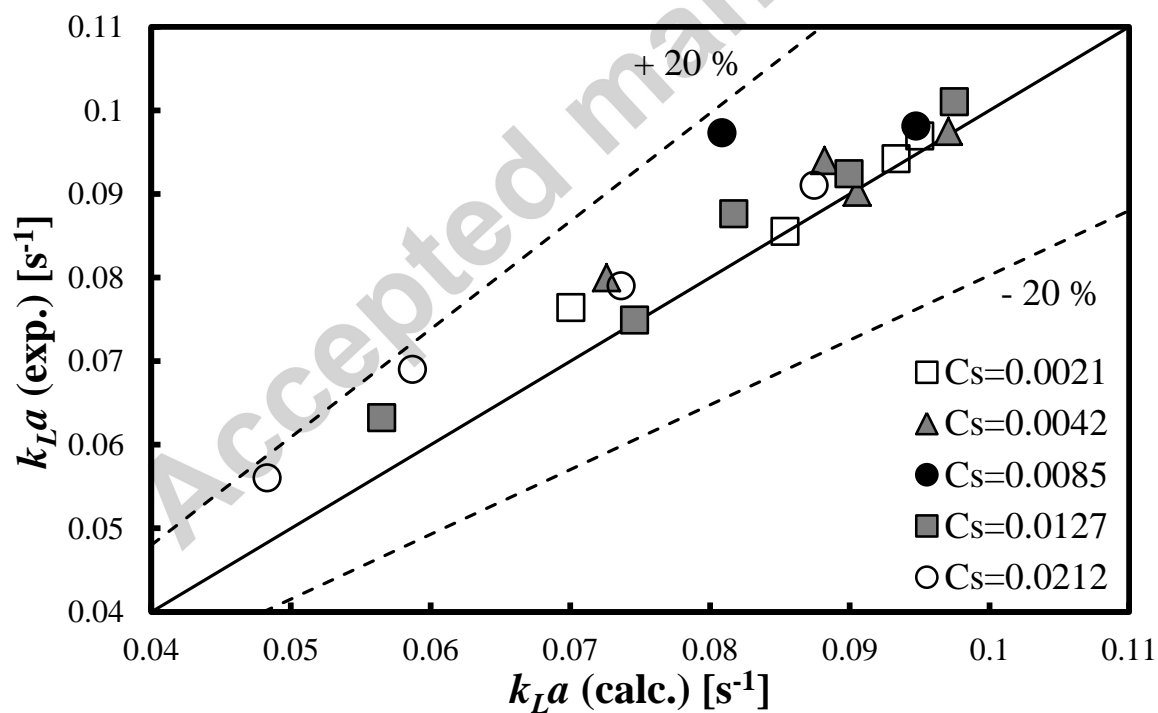

Fig. 11. Parity plot of k_La values in a slurry bubble column operated with air-Na$_2$SO$_4$-kieselguhr system.

In **Tables 6a** and **b** are listed the ranges of the main parameters corresponding to the points in Figs. 8-11. The modification of the contact time in slurry bubble columns is applicable for d_s values between 4.107 and 5.689 mm, l values between 4.712 and 6.511 mm, h values between 3.121 and 4.344 mm, Re_b values between 325.988 and 1088.860, Ta values between 3.878 and 4.858 as well as Eo values between 2.872 and 5.622.

Table 6a. Bubble size and its geometrical characteristics in four different three-phase systems.

Liquid-Solid System	C_s [-]	d_s [mm]	l [mm]	h [mm]
Tetralin-Alumina	0.0045	4.120-4.254	4.712-4.894	3.150-3.215
Tetralin-Alumina	0.013	4.127-4.262	4.727-4.911	3.147-3.211
Tetralin-Alumina	0.0281	4.107-4.241	4.712-4.895	3.121-3.185
Tetralin-Alumina	0.0433	4.160-4.296	4.790-4.976	3.138-3.201
Water-Alumina	0.0031	4.782-4.921	5.367-5.549	3.798-3.871
Water-Alumina	0.0157	4.864-5.002	5.476-5.659	3.838-3.910
Water-Alumina	0.0314	4.994-5.118	5.651-5.816	3.902-3.965
Water-Alumina	0.0472	4.703-5.166	5.280-5.888	3.734-3.978
Water-Alumina	0.0629	5.108-5.350	5.817-6.133	3.941-4.071
Water-Activated carbon	0.0051	4.575-4.714	5.094-5.275	3.691-3.767
Water-Activated carbon	0.0256	4.772-5.029	5.341-5.670	3.811-3.957
Water-Activated carbon	0.0383	5.017-5.382	5.645-6.117	3.964-4.167
Water-Activated carbon	0.0511	4.990-5.689	5.600-6.511	3.962-4.344
Na_2SO_4-Kieselguhr	0.0021	4.940-5.010	5.585-5.678	3.866-3.902
Na_2SO_4-Kieselguhr	0.0042	5.054-5.005	5.667-5.732	3.905-3.930
Na_2SO_4-Kieselguhr	0.0085	5.079-5.093	5.762-5.781	3.946-3.953
Na_2SO_4-Kieselguhr	0.0127	5.120-5.192	5.815-5.911	3.970-4.006
Na_2SO_4-Kieselguhr	0.0212	5.270-5.359	6.010-6.127	4.054-4.101

Table 6b. Three important dimensionless numbers in four different three-phase systems.

Liquid-Solid System	C_s [-]	Re_b [-]	Ta [-]	Eo [-]
Tetralin-Alumina	0.0045	374.596-387.405	4.516-4.670	4.760-5.075
Tetralin-Alumina	0.013	363.448-375.995	4.554-4.711	4.867-5.191
Tetralin-Alumina	0.0281	354.705-367.003	4.595-4.754	4.980-5.310
Tetralin-Alumina	0.0433	325.988-337.432	4.693-4.858	5.273-5.622
Water-Alumina	0.0031	1059.810-1088.860	4.055-4.166	3.127-3.312

Water-Alumina	0.0157	960.883-987.107	4.131-4.244	3.324-3.516
Water-Alumina	0.0314	847.094-867.693	4.247-4.351	3.621-3.803
Water-Alumina	0.0472	766.517-832.524	4.060-4.426	3.316-4.000
Water-Alumina	0.0629	684.052-720.693	4.403-4.577	4.033-4.423
Water-Activated carbon	0.0051	955.903-982.772	3.878-3.987	2.872-3.050
Water-Activated carbon	0.0256	762.758-803.318	3.992-4.162	3.176-3.526
Water-Activated carbon	0.0383	592.429-652.296	4.115-4.357	3.544-4.077
Water-Activated carbon	0.0511	480.234-558.425	4.057-4.534	3.540-4.601
Na_2SO_4-Kieselguhr	0.0021	908.282-920.802	4.227-4.286	3.538-3.639
Na_2SO_4-Kieselguhr	0.0042	864.265-872.526	4.264-4.305	3.640-3.712
Na_2SO_4-Kieselguhr	0.0085	828.508-830.769	4.316-4.328	3.767-3.788
Na_2SO_4-Kieselguhr	0.0127	786.987-797.932	4.339-4.399	3.846-3.955
Na_2SO_4-Kieselguhr	0.0212	704.297-710.393	4.439-4.505	4.115-4.254

4.2.1 Role of the correction factor in slurry bubble columns

It was found that when the predicted k_La values in a slurry bubble column are multiplied by the inverse value of f_c (see Eq. **(17)**) the relative errors (RE) improve with about 5 %. In the definition of Re_b (see Eq. **(6)**) the liquid density is substituted by the slurry density and the liquid viscosity is substituted by the effective viscosity. The results for two different gas-liquid-solid systems are listed in **Table 7**. The f_c^{-1} values are slightly higher than 1. There are only few exceptions in the case of air-Na_2SO_4-kieselguhr system (C_s=0.0021, U_g=0.0483 ms^{-1}; C_s=0.0021, U_g=0.0571 ms^{-1}; C_s=0.0021, U_g=0.0666 ms^{-1}; C_s=0.0042, U_g=0.0488 ms^{-1}; C_s=0.0042, U_g=0.0666 ms^{-1}; C_s=0.0127, U_g=0.0409 ms^{-1}; C_s=0.0127, U_g=0.0577 ms^{-1}) where the correction factor is in fact not needed.

Table 7. Effect of the correction factor on the improvement of the k_La values in a slurry bubble column operated with two different three-phase systems.

Liquid-solid system	C_s [-]	U_g [m/s]	1/f_c [-]	RE [%] (with 1/f_c)	RE [%] (without 1/f_c)
Water-Alumina	0.0031	0.0172	1.0481	13.56	17.53
	0.0031	0.0268	1.0483	3.89	8.32
	0.0031	0.0347	1.0485	1.33	5.89
	0.0031	0.0503	1.0486	4.43	8.86
	0.0031	0.0655	1.0488	0.88	5.49
	0.0031	0.0721	1.0488	3.19	7.69

Water-Alumina	0.0157	0.0179	1.0507	5.26	9.83
	0.0157	0.0268	1.0509	8.22	12.67
	0.0157	0.0330	1.0510	10.95	15.21
	0.0157	0.0488	1.0512	15.42	19.54
	0.0157	0.0629	1.0514	16.07	20.17
	0.0157	0.0729	1.0515	10.33	14.72
Water-Alumina	0.0314	0.0188	1.0544	16.55	20.85
	0.0314	0.0268	1.0546	17.93	22.18
	0.0314	0.0348	1.0547	19.79	23.94
	0.0314	0.0518	1.0550	20.00	24.16
	0.0314	0.0641	1.0551	19.00	23.23
Water-Alumina	0.0472	0.0188	1.0566	10.11	14.93
	0.0472	0.0267	1.0563	4.45	9.88
	0.0472	0.0342	1.0582	1.43	4.43
	0.0472	0.0515	1.0558	0.42	5.85
	0.0472	0.0558	1.0574	1.01	4.56
	0.0472	0.0638	1.0556	6.71	11.73
Water-Alumina	0.0629	0.0188	1.0619	13.47	19.43
	0.0629	0.0267	1.0614	9.38	14.62
	0.0629	0.0347	1.0608	0.83	6.52
	0.0629	0.0515	1.0605	1.57	7.19
	0.0629	0.0637	1.0602	9.54	14.67
Na_2SO_4-Kieselguhr	0.0021	0.0404	1.0528	3.46	8.30
	0.0021	0.0483	1.0529	5.13	0.15
	0.0021	0.0571	1.0530	4.31	0.94
	0.0021	0.0666	1.0530	3.26	1.94
Na_2SO_4-Kieselguhr	0.0042	0.0409	1.0542	4.34	9.26
	0.0042	0.0488	1.0543	5.83	0.38
	0.0042	0.0577	1.0544	1.06	6.17
	0.0042	0.0666	1.0545	4.97	0.45
Na_2SO_4-Kieselguhr	0.0085	0.0484	1.0557	12.26	16.88
	0.0085	0.0556	1.0558	1.94	3.41
Na_2SO_4-Kieselguhr	0.0127	0.0332	1.0569	5.49	10.58
	0.0127	0.0409	1.0570	5.30	0.39

	0.0127	0.0488	1.0183	5.03	6.73
	0.0127	0.0577	1.0572	2.94	2.63
	0.0127	0.0666	1.0573	2.07	3.47
Na$_2$SO$_4$-Kieselguhr	0.0212	0.0332	1.0609	8.46	13.72
	0.0212	0.0409	1.0608	9.71	14.92
	0.0212	0.0488	1.0607	1.13	6.78
	0.0212	0.0577	1.0606	1.95	3.89

4.3. Alternative approach for k_La prediction in a slurry bubble column

The key step in the prediction of the k_La coefficients in slurry bubble columns is the accurate estimation of the mean bubble diameter d_b. Since there is no reliable correlation for its prediction, it can be assumed that d_b is proportional to the length scale of the micro eddies l_e. As an initial approximation, it is assumed that the constant of proportionality is equal to 100. The l_e values can be estimated from the correlation of Deckwer (1980):

$$l_e = \left(\frac{\nu_{SL}^3}{\in} \right)^{0.25} \tag{18}$$

where slurry kinematic viscosity can be calculated as follows:

$$\nu_{SL} = \frac{\mu_{eff}}{\rho_{SL}} \tag{18a}$$

The energy dissipation rate per unit mass can be estimated as follows:

$$\in = g\, U_g \tag{18b}$$

The bubble rise velocity in a slurry bubble column can be also calculated by the correlation of Luo et al. (1997):

$$u_b = \sqrt{\frac{2.8\sigma}{\rho_{SL} d_b} + 4.905 \left(\frac{\rho_{SL} - \rho_G}{\rho_{SL}} \right) d_b} \tag{19}$$

The gas-liquid contact time is a ratio of the mean bubble diameter d_b to the bubble rise velocity u_b. The theoretical k_La values are calculated from Eq. (1). It is assumed that the theoretically calculated k_La values should be multiplied by a proportionality constant since the relationship between d_b and l_e implies such a constant. The constant is derived based on the fit between the experimental k_La values and the theoretically predicted ones. In other words, in the next figures the theoretical k_La values are calculated as a product between the ones calculated based on the above-described algorithm and a constant of 0.9507.

30

Fig. 12 shows that in the case of air-water-alumina system the predicted k_La values based on the length of the micro eddies are close to the experimental k_La values. The new concept is applicable up to solids concentrations C_s of 6.29 %.
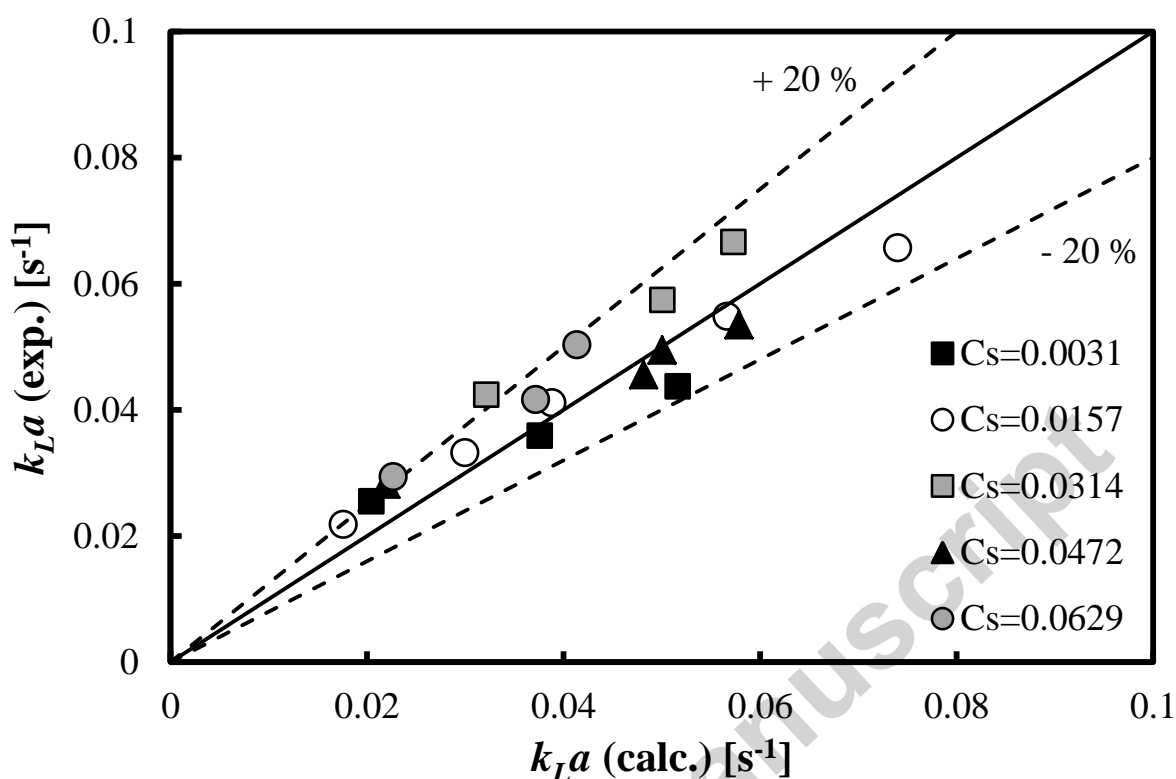

Fig. 12. Comparison between the experimental k_La values and the ones calculated on the basis of the length of micro eddies in a slurry bubble column operated with air-water-alumina system.

In the case of air-water-activated carbon system (see **Fig. 13**) only the k_La data at three different solid concentrations C_s can be fitted successfully based on the new concept.
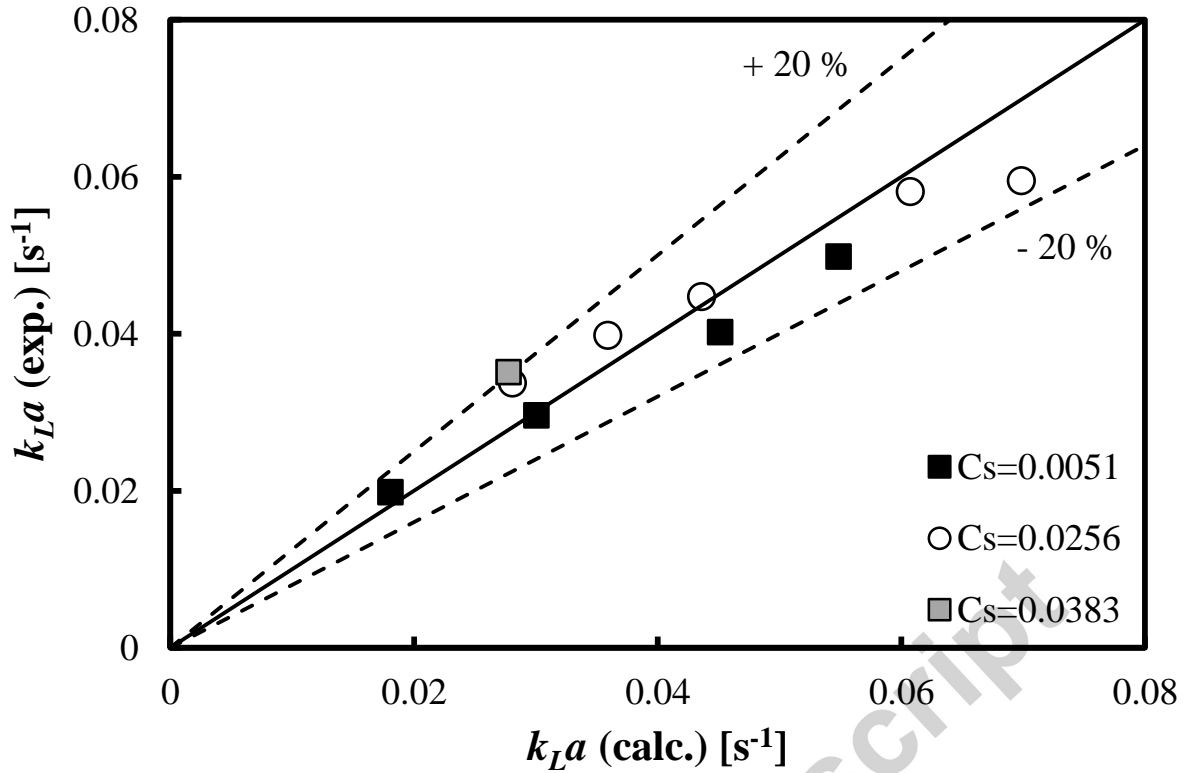
31

Fig. 13. Comparison between the experimental $k_L a$ values and the ones calculated on the basis of the length of micro eddies in a slurry bubble column operated with air-water-activated carbon system.

In **Table 8** is provided a comparison for both three-phase systems between the bubble diameters calculated from Eq. (12) and the ones calculated by means of the length of the micro eddies. It is clear that the differences are not essential.

Table 8. Comparison between the mean bubble diameters calculated by Eq. (12) and the ones estimated from the length scale of the micro eddies in two three-phase systems.

Liquid-solid system	C_s [-]	U_g [m/s]	Eq. (12)	$100 l_e$
Water-Alumina	0.0031	0.0172	d_b=4.921 mm	d_b=5.104 mm
		0.0268	d_b=4.878 mm	d_b=4.568 mm
		0.0347	d_b=4.852 mm	d_b=4.282 mm
	0.0157	0.0179	d_b=5.002 mm	d_b=5.473 mm
		0.0268	d_b=4.962 mm	d_b=4.948 mm
		0.033	d_b=4.942 mm	d_b=4.698 mm
		0.0488	d_b=4.903 mm	d_b=4.260 mm
		0.0629	d_b=4.878 mm	d_b=3.998 mm
	0.0314	0.0348	d_b=5.055 mm	d_b=5.158 mm
		0.0518	d_b=5.015 mm	d_b=4.670 mm

		0.0641	d_b=4.944 mm	d_b=4.728 mm
	0.0472	0.0267	d_b=5.106 mm	d_b=5.743 mm
		0.0515	d_b=4.996 mm	d_b=4.731 mm
		0.0558	d_b=4.703 mm	d_b=4.620 mm
		0.0638	d_b=4.961 mm	d_b=4.440 mm
	0.0629	0.0347	d_b=5.254 mm	d_b=6.075 mm
		0.0515	d_b=5.150 mm	d_b=5.373 mm
		0.0637	d_b=5.108 mm	d_b=5.030 mm
Water-Activated carbon	0.0051	0.0160	d_b=4.720 mm	d_b=5.465 mm
		0.0234	d_b=4.684 mm	d_b=4.970 mm
		0.0317	d_b=4.656 mm	d_b=4.607 mm
		0.0395	d_b=4.636 mm	d_b=4.360 mm
	0.0256	0.0316	d_b=4.905 mm	d_b=5.618 mm
		0.0395	d_b=4.867 mm	d_b=5.253 mm
		0.0477	d_b=4.834 mm	d_b=4.963 mm
		0.0641	d_b=4.809 mm	d_b=4.541 mm
		0.0716	d_b=4.798 mm	d_b=4.392 mm
	0.0383	0.0477	d_b=5.074 mm	d_b=5.942 mm

5. Conclusion

The results in this paper demonstrated that with an appropriate definition of the gas-liquid contact time (Nedeltchev et al., 2007; Nedeltchev et al., 2014) the penetration theory can be applied successfully not only to gas-liquid bubble columns but also to slurry bubble columns. When the contact time was defined as a ratio of bubble surface to the rate of surface formation, the volumetric liquid-phase mass transfer coefficients k_La were predicted successfully in a bubble column (0.095 m in ID) operated with an air and the following ten liquids: decalin, 1,2-dichloroethane, 1,4-dioxane, ethanol (99 %), ethylene glycol, nitrobenzene, 2-propanol, tetralin, water and xylene. The k_La predictions in two liquid mixtures were also quite good. In a slurry bubble column (0.095 m in ID) the k_La values were predicted successfully in the following four liquid-solid systems: tetralin-alumina, water-alumina, water-activated carbon and sodium sulphate-kieselguhr. It was found that in some cases the penetration theory is applicable up to solids concentrations of 6.29 %.

It is noteworthy that in both gas-liquid and slurry bubble columns the penetration theory was found applicable up to superficial gas velocities of 0.08 m/s. In other words, the new

definition of the contact time renders the theory applicable not only in the homogeneous regime but also in the heterogeneous regime.

It was found that when the theoretically predicted $k_L a$ values are multiplied by the correction factor introduced earlier by Lochiel and Calderbank (1964), the $k_L a$ predictions improve in some organic liquids (1,2-dichloroethane, ethanol (99 %) and xylene) and liquid mixture (toluene-ethanol 97.2 %). In the case of a slurry bubble column, a multiplication of each theoretical $k_L a$ value with the reverse value of the correction factor f_c improves the predictions with about 5 %. This result was demonstrated in the case of two liquid-solid systems: water-alumina and Na_2SO_4-kieselguhr.

Finally, the bubble diameters in two slurry systems (air-water-alumina and air-water-activated carbon) have been calculated from the length scales of the micro eddies and then the new definition of the contact time has been applied for a successful prediction of the $k_L a$ values. This is also a very promising approach.

Acknowledgment

References

Akita, K., Yoshida, F., 1973. Gas hold-up and volumetric mass transfer coeficients in bubble columns. Ind. Eng. Chem. Process Des. Dev. 12, 76-80.

Akita, K., Yoshida, F., 1974. Bubble size, interfacial area, and liquid-phase mass transfer coefficients in bubble columns. Ind. Eng. Chem. Proc. Des. Dev. 13, 84-91.

Alvarez-Cuenca, M., Baker, C. G. J., Bergougnou, M. A., 1980. Oxygen mass transfer in bubble columns. Chemical Engineering Science 35, 1121-1127.

Alvarez-Cuenca, M., M. A. Nerenberg, 1981. Oxygen mass transfer in bubble columns working at large gas and liquid flow rates. AIChE Journal 27, 66-73.

Braulick, W. J., Fair, J. R., Lerner, B. J., 1965. Mass transfer in a sparged contactor: part I. physical mechanisms and controlling parameters. AIChE Journal 11, 73-79.

Calderbank, P. H., Moo-Young, M. B., 1961. The continuous phase heat and mass transfer properties of dispersions. Chemical Engineering Science 16, 39-54.

Calderbank, P. H., 1967. Gas absorption from bubbles. The Chemical Engineer 45, CE209-CE233.

Calderbank, P. H., Johnson, D. S. L., Loudon, J., 1970. Mechanics and mass transfer of single bubbles in free rise through some Newtonian and non-Newtonian liquids. Chemical Engineering Science 25, 235-256.

Chao, B. T., 1962. Motion of spherical gas bubbles in a viscous liquid at large Reynolds numbers. The Physics of Fluids 5, 69-79.

Clift, R., Grace, J. R., Weber, M., 1978. Bubbles, Drops and Particles, first edition. Academic Press, New York, NY.

Deckwer, W.-D., Adler, I., Zaidi, A., 1978. A comprehensive study on CO_2-interphase mass transfer in vertical cocurrent and countercurrent gas-liquid flow. The Canadian Journal of Chemical Engineering 56, 43-55.

Deckwer, W.-D., 1980. On the mechanism of heat transfer in bubble column reactors. Chemical Engineering Science 35, 1341-1346.

Deckwer, W.-D., Nguyen-tien, K., Godbole, B., Shah, Y. T., 1983. Applicability of axial dispersion model to analyze mass transfer measurements in bubble columns. AIChE Journal 29, 915-922.

Deckwer, W.-D., Schumpe, A., 1993. Improved tools for bubble column reactor design and scale-up. Chemical Engineering Science 48, 889-911.

Fan, L.-S., Tsuchiya, K., 1990. Bubble Wake Dynamics in Liquids and Liquid-Solid Suspensions, first edition. Butterworth-Heinemann Series in Chemical Engineering. Stoneham, USA.

Garcia-Ochoa, F., Gomez, E., 2004. Theoretical prediction of gas-liquid mass transfer coefficient, specific area and hold-up in sparged stirred tanks. Chemical Engineering Science 59, 2489-2501.

Godbole, S. P., Schumpe, A., Shah, Y. T., 1983. Chemical Engineering Communications 24, 235-258.

Higbie, R., 1935. The rate of absorption of a pure gas into a still liquid during short periods of exposure. Trans. A.I.Ch.E. 31, 365-389.

Hikita, H., Asai, S., Tanigawa, K., Segawa, K., Kitao, M., 1981. The volumetric mass transfer coefficient in bubble columns. Chemical Engineering Journal 22, 61-67.

Kawase, Y., Halard, B., Moo-Young, M., 1987. Theoretical prediction of volumetric mass transfer coefficients in bubble columns for Newtonian and non-Newtonian fluids. Chemical Engineering Science 42, 1609-1617.

Kolbel, H., Ralek, M., 1980. The fischer tropsch synthesis in the liquid phase. Catal. Rev. Sci. Eng. 21, 255-274.

35

Krishna, R., De Swart, J. W. A., Hennephof, D., Ellenberger, J., Hoefsloot, H. C. J., 1994. Influence of increased gas density on hydrodynamics of bubble column reactors. AIChE Journal 40, 112-119.

Lemoine, R., Morsi, B. I., 2005. An algorithm for prediction the hydrodynamic and mass transfer parameters in agitated reactors. Chemical Engineering Journal 114, 9-31.

Lemoine, R., Behkish, A., Sehabiague, L., Heintz, Y. J., Oukaci, R., Morsi, B. I., 2008. An algorithm for predicting the hydrodynamic and mass transfer parameters in bubble column and slurry bubble column reactors. Fuel Processing Technology 89, 322-343.

Lochiel, A. C., Calderbank, P. H., 1964. Mass transfer in the continuous phase around axisymmetric bodies of revolution. Chemical Engineering Science 19, 471-484.

Luo, X., Zhang, J., Tsuchiya, K., Fan, L.-S., 1997. On the rise velocity of bubbles in liquid-solid suspensions at elevated pressure and temperature. Chemical Engineering Science 52, 3693- 3699.

Martín, M., Montes, F. J., Galán, M. A., 2009. Physical explanation of the empirical coefficients of gas-liquid mass transfer equations. Chemical Engineering Science 64, 410-425.

Mendelson, H. D., 1967. The prediction of bubble terminal velocities from wave theory. AIChE Journal 13, 250-253.

Nakanoh, M., Yoshida, F., 1980. Gas absorption by Newtonian and non-Newtonian liquids in a bubble column. Ind. Eng. Chem. Proc. Des. Dev. 19, 190-195.

Nedeltchev, S., Ookawara, S., Ogawa, K., 2003. Quality of mixedness profiles based on spatial distribution of local mass transfer coefficients in a bubble column. Canadian Journal of Chemical Engineering 81, 597-603.

Nedeltchev, S., Jordan, U., Schumpe, A., 2007. Correction of the penetration theory based on mass transfer data from bubble columns operated in the homogeneous regime under high pressure. Chemical Engineering Science 62, 6263-6273.

Nedeltchev, S., Nigam, K. D. P., Schumpe, A., 2014. Prediction of mass transfer coefficients in a slurry bubble column based on the geometrical characteristics of bubbles. Chemical Engineering Science 106, 119-125.

Öztürk, S. S., Schumpe, A., 1987. The influence of suspended solids on oxygen transfer to organic liquids in a bubble column. Chemical Engineering Science 42, 1781-1785.

Öztürk, S. S., Schumpe, A., Deckwer, W.-D., 1987. Organic liquids in a bubble column: hold-ups and mass transfer coefficients. AIChE Journal 33, 1473-1480.

Painmanakul, P., Loubière, K., Hèbrard, G., Mietton-Peuchot, Roustan, M., 2005. Effect of surfactants on liquid-side mass transfer coefficients. Chemical Engineering Science 60, 6480-6491.

Saxena, S. C., 1995. Bubble column reactors and fischer-tropsch synthesis. Catal. Rev. Sci. Eng. 37, 227-309.

Sauer, T., Hempel, D.-C., 1987. Fluid dynamics and mass transfer in a bubble column with suspended particles. Chemical Engineering and Technology 10, 180-189.

Schumpe, A., Serpemen, Y., Deckwer, W.-D., 1979. Effective application of bubble columns. German Chemical Engineering 2, 234-241.

Schumpe, A., Deckwer, W.-D., 1987. Viscous media in tower bioreactors: hydrodynamic characteristics and mass transfer properties. Bioprocess Engineering 2, 79-94.

Shah, Y. T., Kelkar, B. G., Godbole, S. P., Deckwer, W.-D., 1982. Design parameter estimations for bubble column reactors. AIChE J. 28, 353-379.

Suh, I.-S., Schumpe, A., Deckwer, W.-D., Kulicke, W.-M., 1991. Gas liquid mass transfer in the bubble column with viscoelastic liquid. Canadian Journal of Chemical Engineering 69, 506-512.

Tarmy, B. L., Chang, M., Coulaloglou, C. A., Ponzi, P. R., 1984. The three phase hydrodynamic characteristics of the EDS coal liquefaction reactors: their development and scale-up. Proceedings of the Eight International Symposium on Chemical Reaction Engineering, Elsevier Scientific, NY.

Terasaka, K., Inoue, Y., Kakizaki, M., Niwa, M., 2004. Simultaneous measurement of 3-dimensional shape and behavior of single bubble in liquid using laser sensors. Journal of Chemical Engineering of Japan 37, 921-926.

Thorat, B. N., Shevade, A. V., Bhilegaonkar, K. N., Aglawe, R. H., Parasu Verra, U., Thakre, S. S., Pandit, A. B., Sawant, S. B., Joshi, J. B., 1998. Effect of sparger design and height to diameter ratio on fractional gas holdup in bubble columns. Trans. Inst. Chem. Eng. 76 (Part A), 823-834.

Wang, T., Wang, J., 2007. Numerical simulations of gas-liquid mass transfer in bubble columns with a CFD-PBM coupled model. Chemical Engineering Science 62, 7107-7118.

Weber, M. E., 1975. The effect of surface active agents on mass transfer from spherical cap bubbles. Chemical Engineering Science 30, 1507-1510.

Wilkinson, P. M., Haringa, H., Van Dierendonck, L. L., 1994. Mass transfer and bubble size in a bubble column under pressure. Chemical Engineering Science 49, 1417-1427.

Zhao, M., Niranjan, K., Davidson, J. F., 1994. Mass transfer to viscous liquids bubble columns and air lift reactors: influence of baffles. Chemical Engineering Science 49, 2359-2369.

Highlights

- New definition of gas-liquid contact time.
- Applicability range of the modified penetration theory.
- Role of the correction factor.
- Operation of a gas-liquid bubble column with organic liquids.
- Operation of a slurry bubble column with four different systems.